Towards an Understanding of BACE1 Activity in the Occurrence of Vascular Dementia

Melanie Jane Taylor

Submitted in accordance with the degree of Master of Science by Research

The University of Leeds

School of Medicine

December 2020

Declarations

The candidate confirms that the work submitted is her own and that appropriate credit has been given where reference has been made to the work of others.

Acknowledgments

Firstly, I would like to thank my supervisor Dr Paul Meakin for agreeing to take me on as a master's student and offering me support and guidance throughout what has been a difficult year.

This research was carried out in conjunction with Jane Brown who performed the peripheral endothelial cell isolations, stimulations and harvests. Jane also performed a portion of the western blots on the peripheral endothelial cell isolations. My own contributions, fully and explicitly indicated in the thesis, have been completion of the peripheral endothelial cell western blots, isolation, stimulation and analysis by western blot of brain endothelial cell isolations, piloting of the brain endothelial cell angiogenic bead assay and all computational simulations.

Further to this, I would like to thank Jane brown for her patient and meticulous demonstration of laboratory techniques and always being available to answer questions.

I would also like to thank Dr Nicole Watt for teaching me the procedure for the isolation of brain endothelial cells. Additionally, I must thank Eva Clavane for demonstrating the angiogenic bead assay and for being a source of support and encouragement throughout my time at LICAMM.

Lats but not least I would like to thank my husband, John Taylor, for his long enduring patience, his unfaltering encouragement and his endless ability to step up and provide practical support, whether that be childcare or cooking tea when I'm exhausted.

Abstract

Background: Vascular dementia is the second most prolific form of dementia after Alzheimer's disease and is hallmarked by cognitive decline. Currently, there is no direct treatment for vascular dementia. Previous works have pointed towards links between vascular dementia, insulin resistance and endothelial dysfunction. BACE1 has recently been shown to cleave the insulin receptor, potentially driving insulin resistance. Subsequently, insulin resistance is characterised by an imbalance between vasoactive compounds ET-1 and nitric oxide synthase, leading to endothelial dysfunction.

Objective: Here we examine the impact of the modulation of BACE1 activity on the insulin stimulated Akt and eNOS signalling pathway in the endothelium, in order to assess the contribution of BACE1 to endothelial dysfunction.

Methods: Murine peripheral and brain endothelial cells were isolated from wild type and BACE1 knockout mice, with a portion of wildtype cells being treated with a BACE1 inhibitor. Cells were stimulated with insulin before cellular protein content was harvested and analysed by western blot for changes in Akt and eNOS activity.

Results: Phosphorylation of eNOS and Akt was increased when BACE1 was inhibited genetically or pharmacologically in peripheral murine endothelial cells. Genetic knockout of BACE1 contributed significantly to increases eNOS phosphorylation ($P = 0.0276$). With pharmacological inhibition of BACE1 also making significant contributions to eNOS phosphorylation ($P = 0.0001$). However, the same signalling differences in murine brain endothelial cells were not clearly observed. This is likely due to the lack of data available for this cell line.

Conclusion: Such demonstrable improvements suggest BACE1 may be a suitable target for the treatment and management of peripheral diseases with underlying endothelial dysfunction. Should results in BECs follow the same pattern of improved Akt and eNOS phosphorylation then BACE1 may considered as a plausible drug target for the treatment of cerebrovascular impairments.

Table of Contents

List of Figures

List of Tables

List of Abbreviations

AA	Amino Acid
AD	Alzheimer’s
APP	Amyloid Precursor Protein
Aβ	Beta-Amyloid
BACE1	β-site Amyloid Precursor Protein Cleaving Enzyme 1
BBB	Blood Brain Barrier
BECs	Brain Endothelial Cells
BSA	Bovine Serum Albumen
CI	Confidence Interval
CSF	Cerebral Spinal Fluid
CSF	Cerebral Spinal Fluid
DMEM	Dubeccos's Modified Eagle's Medium
ECs	Endothelial Cells
eNOS	Endothelial Nitric Oxide Synthase
ET-1	Endothelin-1
GLUT-4	Glucose Transport Protein-4
HBSS	Hanks' Balanced Salt Solution
HIF-1α	Hypoxia-Inducible Factor 1α
IR	Insulin Receptor
IRS1	Insulin Receptor Substrate 1
L-NAME	N^{ω}-nitro L-arginine methyl ester
MIC	Multi Infarct Dementia
NCBI	National Centre for Biotechnology Information
NO	Nitric Oxide
NVU	Neuro Vascular Unit

P-Akt	Phosphorylated Akt
PBS	Phosphate Buffer Saline
PDB	Protein Data Bank
P-eNOS	Phosphorylated eNOS
PSD	Post Stroke Dementia
RMSD	Root Mean Square Deviation
ROS	Reactive Oxygen Species
SEM	Standard Error of the Mean
T2DM	Type 2 Diabetes Mellitus
VaD	Vascular dementia
VCI	Vascular cognitive impairment
VEGF R-1	Vascular Endothelial Growth Factor Receptor-1

1. Graphical Abstract

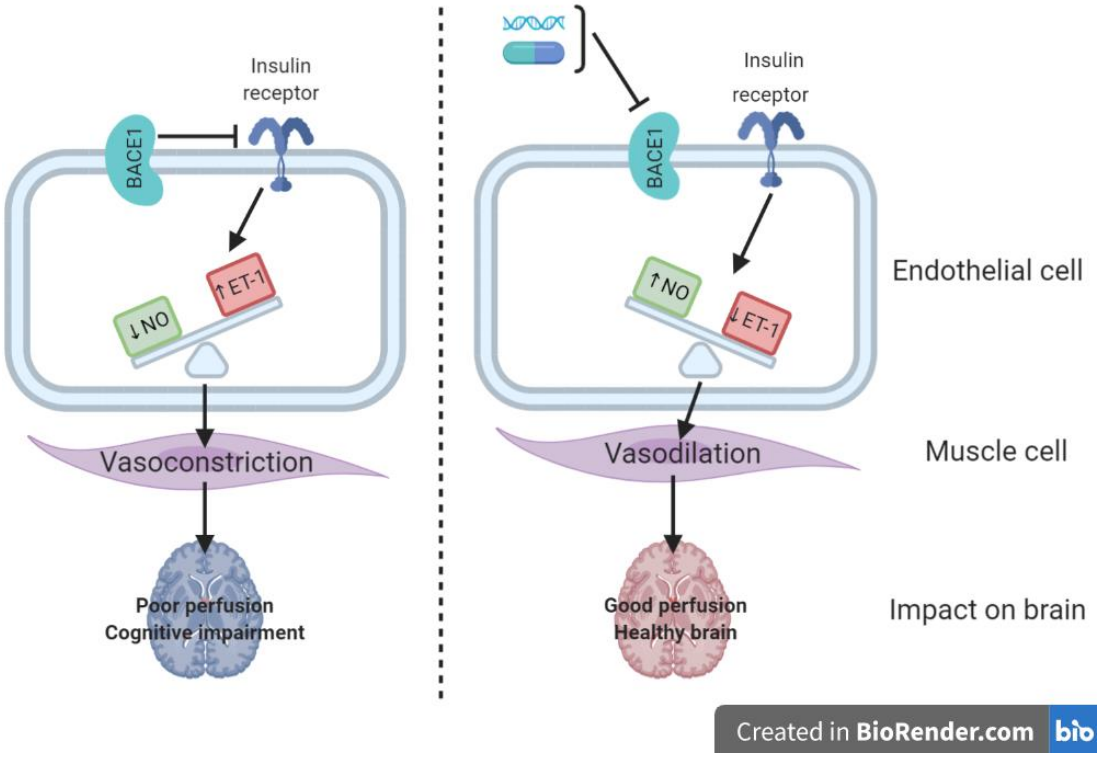

Figure 1: Modulation of BACE1 activity and its impact on endothelial health. BACE1 inhibits endothelial insulin signalling causing imbalance between NO and ET-1 which leads to endothelial dysfunction and vasoconstriction. Subsequently, cerebral perfusion is impaired and can cause vascular dementia. Inhibition of BACE1 helps recover the imbalanced NO and ET-1 signalling leading to vasodilation and improved cerebral perfusion, protecting the brain against cognitive impairments.

2. Introduction

2.1. Vascular dementia

2.1.1. An overview

Vascular dementia (VaD) is one of the most prolific forms of dementia; it is second only to Alzheimer's (AD) (O'Brien and Thomas, 2015), accounting for approximately 15 – 30% of all dementia cases (van der Flier et al, 2018). Furthermore, approximately 20% - 40% of AD cases present with mixed VaD pathology; that is, they display vascular pathologies alongside traditional AD pathologies (Zerky et al, 2002). The most common risk factor for VaD is age and as the population in western communities continues to age the burden represented by VaD is expected to double by 2050 (Livingston et al, 2017). Such a surge in prevalence would no doubt lead to increased economic strain and pressure on the NHS; demonstrated by the 31% prevalence increase alongside the 35% cost of care increase seen between 2010 and 2015 (Wimo et al, 2017). In addition to the economic impact of increased VaD prevalence, the human cost should also be considered. VaD is characterised by cognitive impairment which can affect functions such as memory and motor skills, often leaving sufferers vulnerable and reliant on the care of others.

2.1.2. A brief history of dementia

Cognitive impairments have been associated with cerebral vascular pathology as early as the Seventeenth century, when Bayle attributed these impairments to "a failure of the influx of blood to the brain" (Girouard and Munter,2018). Modern theories regarding VaD began to emerge during the late-nineteenth century when a number of contemporaries in the field of neuroscience described the heterogenic nature of vascular pathologies linked with cognitive decline (Roman, 2003). During this time Binswanger described a pattern of atherosclerosis of cerebral arteries in conjunction with widespread white matter damage. Further to this, Alzheimer

recognised the existence of neuro degeneration with little or no evidence of vascular pathology and called for distinction between the aetiologies. Developing his research further, Alzheimer noted that the presence of vascular pathologies only, resulted in milder cognitive impairments. Following on from this, a textbook by Kraepelin illustrated various vascular pathologies that corelated with senility (Roman, 1999) (Wolters and Ikram, 2019).

The late-twentieth century saw AD become the most prolific form of dementia diagnosed and as such vast amounts of research went into deciphering the underlying mechanism. Currently, it is widely accepted that the amyloid cascade theory of AD is one major mechanism by which AD pathologies arise (Karran, Mercken and Strooper, 2011). Another common pathology associated with AD is neurofibril tangles which are generated by hyperphosphorylated tau proteins aggregating (Busche and Hyman, 2020). However, there has been a recent recognition in the field, that as a significant number of AD cases present with vascular pathology, and that such pathologies may play an initiating or potentiating role in the development and onset AD (Kalaria, Akinyemi and Ihara, 2012). The vascular hypothesis of AD describes poor clearance of Aβ from the extracellular space leading to Aβ plaque formation on blood vessel walls (cerebrovascular amyloid angiopathy) inducing cerebral hypoperfusion and subsequent cognitive deficits (Bu, Liu and Kanekiyo, 2013).

2.1.3. Pathological heterogeneity of vascular dementia

Clarity of diagnosis parameters and a sound understanding of molecular mechanisms underpinning the pathophysiology of AD has allowed for better treatment and targeted research in the area. Contrastingly, variation in pathologies and patient symptoms have impaired the development of clear diagnostic guidelines and the unravelling of the driving molecular mechanisms of VaD (Roman et al,

1993). It is only in the last decade that consensus has been built on the classification and diagnostic criterion of vascular cognitive impairments. Both the International Society of Vascular Behavioural and Cognitive Disorders and the American Heart Association have published diagnosis criteria that states that both cognitive impairment and evidence of vascular contribution, usually from imaging, must be present for a diagnosis of vascular cognitive impairment (VCI) (Smith, 2017). VCI can subsequently be classified in terms of severity from mild cognitive impairment, involving only minor alteration to cognitive abilities, to VaD where the level of cognitive impairment impedes on the patient's quality of life (Skrobot et al, 2017).

Confusion regarding the diagnosis of VaD stems from the varied vascular pathologies that can accompany cognitive impairment (Figure 2). Recently a study by Skrobot and colleagues (2017) has attempted to delineate the different subtypes of VaD. Firstly, there is mild VCI which is the presence of cognitive impairment, that does not impede quality of life, with vascular insults. Further to this major VCI or VaD is split into 4 subtypes.

1. Post-stroke dementia (PSD) is diagnosed at around 6 months after a first stroke event where a patient is free of pre-stroke cognitive decline. Diagnosis is carried out at this time point to allow for post-stroke delirium to alleviate. Stroke onset can be either ischemic or haemorrhagic caused by blockade via varying mechanisms or rupture of cerebral blood vessels respectively, leading to reduced blood flow to the surrounding tissues causing cell death (Mok et al, 2017) (CDC, 2020).
2. Subcortical ischemic VaD is characterised by lacunar infarcts that occur in the vasculature of subcortical regions such as the basal ganglia and are usually accompanied by white matter lesions. These structural features must also be accompanied by evidence of cognitive impairment. It has been

suggested that endothelial dysfunction at the cerebral arteriolar level may be an initiating step in pathogenesis (Chui, 2007) (Wardlaw, 2005).

3. Multi infarct dementia (MID) is hallmarked by lesions in both white and grey matter tissues. Occlusion of arteries and arterioles lead to multiple infarcts and subsequent cognitive impairment. MID pathology is commonly present across both cortical and subcortical regions of the brain. Again, endothelial dysfunction has been implicated in the onset of MID (McKay and Counts, 2017) (Thal et al, 2012).
4. Mixed dementia refers to any case of dementia that has hallmarks of more than one clinically recognised dementia. For instance, AD amyloid pathology may be accompanied by vascular pathologies such as lacunar infarcts (Skrobot et al, 2017).

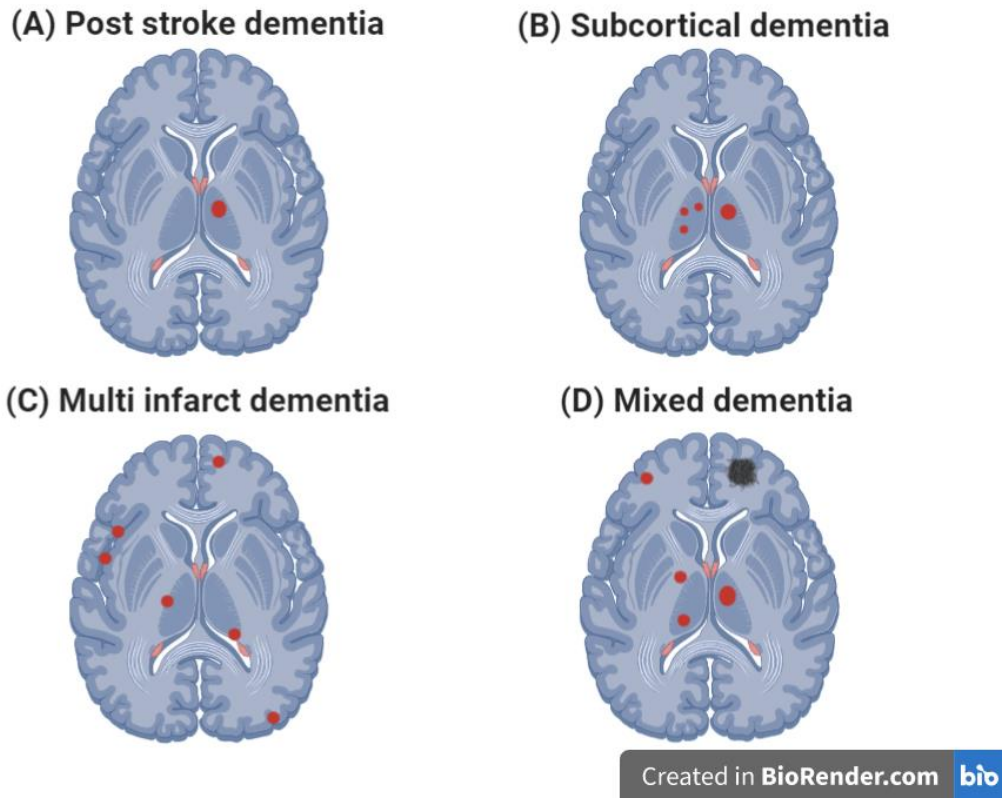

Figure 2: Heterogeneity of pathology in vascular dementia. Red areas denote location and size of vascular insults in the differing contributors to vascular dementia. **(A)** Post stroke dementia can often cause strategic infarcts; that is infarcts to areas of the brain responsible for key functions such as speech. **(B)** Subcortical dementia: vascular insults may be caused by differing mechanisms such as micro bleeds or vessel occlusion, however, insults are isolated in the subcortex. **(C)** Multi infarct dementia is the accumulation of many ischemic events that can occur across all regions of the brain. **(D)** Mixed dementia refers to any vascular pathology in the presence of the pathology of another dementia sub-group, for instance, vascular pathology may co-exist with Aβ plaques.

2.1.4. Treatment of vascular dementia

Currently there are no specific treatments for VaD. This lack of treatments is in part due to the diverse range of pathophysiology's displayed in VaD and the lack of cohesive criterion for its diagnosis. Instead of direct treatment of the disease itself,

management of risk factors is used to slow the progress of the disease. Largely, management of such risk factors involves lifestyle changes including smoking cessation and healthy eating (Ladecola, 2013). In addition, medication may be used to alleviate some risk factors. For instance, the use of statins may be employed to control atherosclerotic damage caused to the vasculature by high cholesterol. Here, statins, targeted to hepatocytes, competitively inhibit HMG-CoA reductase the enzyme responsible for converting HMG-CoA to mevalonate, which is a cholesterol precursor molecule. Inhibition of HMG-CoA reductase results in the truncation of the synthesis pathway and subsequent production of cholesterol (Stancu and Sima, 2001). In addition to statins reducing blood cholesterol levels they also have several pleiotropic effects including increasing the bioavailability of nitric oxide (NO), a vasodilator implicated in the proper function of the endothelium. Such increases in the bioavailability of NO have been demonstrated to have neuro protective effects (Cimino et al, 2007).

2.2. The β-site amyloid precursor protein cleavage enzyme1

2.2.1. BACE1 processing of APP

Since its discovery in 1999 BACE1, also known as β-site Amyloid Precursor Protein Cleaving Enzyme 1, has been synonymous with the onset and development of AD (Araki, 2016). AD is characterised by the presence of amyloid plaques in the brain. BACE1 is responsible for the rate limiting step in the generation of beta-amyloid (Aβ); it is Aβ that subsequently aggregates to form amyloid plaques (Koelsch, 2017). Amyloid precursor protein (APP) is a membrane bound protein that is sequentially cleaved by β and γ secretase enzymes. Proteolytic cleavage of APP by BACE1 initiates the production of Aβ, generating a soluble N-terminus fragment and a transmembrane C-terminus of 99 amino acid residues long (C-99). APP C-99 is subsequently cleaved by γ-secretase, yielding the neurotoxic Aβ fragment

(Christensen et al, 2004) (Figure 3). The embryonic lethality of γ-secretase knockout mice paired with the general health of BACE1 knockout mice and their characteristic lack of Aβ production has led to the targeting of BACE1 in the development of therapeutic agents for AD (Cole and Vassar, 2007). This has sustained an ever-growing pool of knowledge surrounding the function of BACE1.

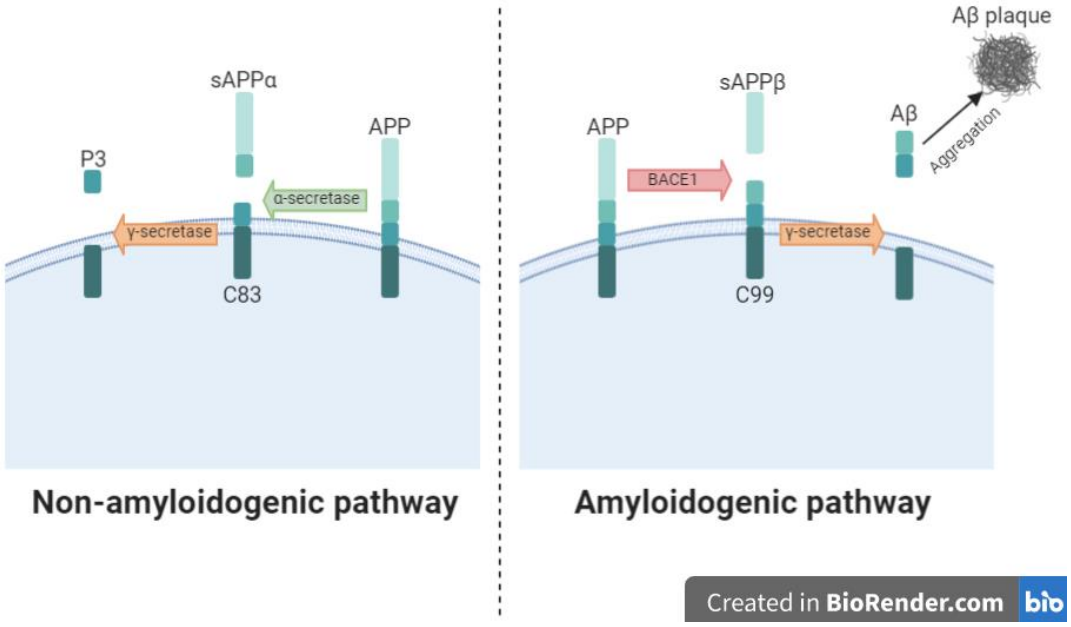

Figure 3: Pathological and non-pathological cleavage pathways of APP. Non-amyloidogenic APP processing results from the cleavage of APP by α-secretase, generating a transmembrane C83 fragment. Subsequent cleavage of C83 by γ-secretase generates the non-toxic P3 fragment. Amyloidogenic APP processing is initiated by BACE1, leaving behind the transmembrane C99 fragment and sAPPβ. C99 is further cleaved by γ-secretase yielding Aβ fragments. Subsequent aggregation of Aβ fragments generates Aβ plaques.

2.2.2. BACE1 Regulation

The gene encoding for BACE1 is located on chromosome 11 and is roughly 30 kilobases in length; it is spread over nine exons. Transcription is highly regulated with numerous promoters and enhancers having been identified (Fishilevich et al,

2017). Such promoters include Sp1 which was shown to bind the BACE1 promoter region to upregulate expression, Sp1 is thought to act in complex with other regulatory elements (Christensen et al, 2004). Another validated promoter of expression is Hypoxia-Inducible Factor 1α (HIF-1α). Here, HIF-1α binds the promotor region of the BACE1 gene in reduced oxygen levels, this is due to the presence of a hypoxia response element in this region, increasing BACE1 expression (Sun et al, 2006). Importantly, it may be noted that cerebral hypoxia is a driver of increased prevalence of both AD and VaD (Zhang et al, 2007). Additionally, post translational modifications such as palmitoylation, phosphorylation and glycosylation are also involved in the regulation of BACE1 activity. For instance, phosphorylated BACE1 demonstrates increased Aβ processing activity and is found in elevated levels in AD brains (Araki, 2016).

2.2.3. BACE1 Isoforms

Alternative splicing of the BACE1 gene has been observed with expression patterns of splice variants differing across tissues and in an age dependent maner. There are four main BACE1 splice variants: BACE1-A, which is 501 amino acids (AA) in length and is considered the canonical form of BACE1, BACE1-B at 476 AA long, BACE1-C with 457 AAs and BACE1-D at 432 AA in length (Holsinger et al, 2013). There are a further two shorter BACE1 isoforms recorded in the UniProt database, termed BACE1-5 and BACE1-6 with chain lengths of 401 and 376 AA respectively (UniProt Consortium, 2019). All four major isoforms contain the BACE1 catalytic residues, however, BACE1-B and BACE1-C show reduced amyloid processing activity compared with BACE1-A. However, this remains a poorly understood aspect of BACE1 function and regulation, exemplified by the lack of further investigations into BACE-D function due to difficulty in amplification of the mRNA (Holsinger et al, 2013).

2.2.4. BACE1 Structure and Function

BACE1 is a membrane bound protein that is part of the aspartic protease superfamily and in contrast to other proteins in this class BACE1 is a transmembrane protein and consists of three domains. The majority of the BACE1 peptide sequence forms the active site containing ectodomain, there is also a transmembrane domain and a small cytoplasmic domain (Koelsch, 2017). The two catalytic aspartic acid motifs ($D^{T}/_{S}G^{T}/_{S}$) positioned at 32 and 228 in the BACE1 amino acid sequence of the mature protein are conserved across the aspartic protease superfamily (Kandalepas and Vassar, 2011). These aspartic acid residues hold a conserved water molecule between them, and this is postulated as being the mechanism by which APP is cleaved at its β-site by a hydrolysis reaction (Shimizu et al, 2008). In addition to the aspartic acid motifs it is thought that the flap region of BACE1 plays a crucial role in its catalytic activities. The flap is a β-hairpin structure that covers the active site, it is a highly flexible region that undergoes significant conformational changes upon substrate binding. Located on the flap is tyrosine 71 which has been demonstrated to be influential in both substrate binding and catalytic activity of BACE1 (Spronk and Carlson, 2011).

Whilst BACE1 has become complicit in the aetiology of AD, it has been shown to demonstrate loose substrate specificity and thus has an ever-increasing list of validated substrates. This suggests functions outside of Aβ production (Barao et al, 2016). Physiological roles for BACE1 include axon guidance and myelination via the cleavage of L1 and neuregulin-1 respectively (Zhou et al, 2012) (Hu et al, 2006).

2.3. Insulin signalling

A primary function of the insulin signalling pathway is to increase cellular uptake of glucose from the blood stream, maintaining blood glucose homeostasis (Choi and

Kim, 2010). Increased blood glucose levels stimulate the release of insulin by the pancreatic β-cells. Subsequently, insulin binds the insulin receptor (IR); a tyrosine kinase receptor. Upon binding a cascade of phosphorylation events is induced accounting for activation of a number of cellular processes (Rains and Jain, 2010). Initially, binding of IR causes phosphorylation of insulin receptor substrate-1 (IRS1) which in turn can phosphorylate multiple proteins in differing branches of the insulin signalling pathways (Zhang and Liu, 2014). One such pathway involves activation of PI-3 Kinase which in turn recruits Akt via PIP3, subsequently activating endothelial nitric oxide synthase (eNOS). eNOS enzymatically converts L-arginine to nitric oxide which mediates vasodilation via the relaxation of vascular smooth muscle fibres (Manrique, Lastra and Sowers, 2015). The PI-3 Kinase, Akt pathway is also responsible for induction of glycogen synthesis and the translocation of the glucose transport protein-4 (GLUT-4) to cell surface membrane where it mediates diffusion of glucose into the cell (Zhang and Liu, 2014). Therefore, this branch of signalling is commonly associated with the metabolic effects of insulin signalling. An alternative branch of the insulin singling pathway is mediated by RAS, MAPK and ERK proteins and is responsible for the mitogenic effects of insulin stimulation such as cell proliferation (Godsland, 2010).

2.3.1. Insulin action in the brain

In addition to its actions in the periphery insulin mediates a variety of functions in the brain such as metabolism, inflammatory response and neurotransmission. For instance, the study of brain-specific IR knockout mice revealed these mice to develop whole body insulin resistance and obesity (Dodd and Tiganis, 2017). Insulin receptors are expressed ubiquitously across the brain, however, there is variation in expression levels across the regions and cell types of the brain with the olfactory bulb, hypothalamus and cerebellum expressing high levels of IR (Plum, Schubert and Bruning, 2005). Insulin receptors are also expressed on the endothelium of the

brain microvasculature. High fat fed induced insulin resistance in rats supressed insulin action in the brain microvasculature impeding perfusion and leading to cognitive impairments (Fu et al, 2017). It is thought that the main source of insulin in the brain is pancreatic insulin that is transported across the blood brain barrier (BBB), as serum levels of insulin correlate with levels detected in cerebral spinal fluid (CSF) (Arnold et al, 2018).

2.3.2. Insulin Receptor Structure

The IR is composed of lumen facing α-subunit that is bound to transmembrane β-subunit via a disulphide linkage, this forms a monomeric unit of IR. A mature IR is a homodimer of this monomeric unit (Croll et al, 2016). The IR homodimer has 2 binding sites for insulin, S1 and S2, which are located α-subunit. Recent crystal structures of IR in complex with insulin show insulin binding between a leucine rich domain of one monomeric unit and the fibronectin type III domain of the other monomeric unit. Comparisons of the empty IR and substrate bound IR structures have been made, demonstrating large scale conformational changes including in the cytoplasmic tyrosine kinase domain, these changes may prove important in signal transduction (Scapin et al, 2018).

2.3.3. Insulin Resistance and Type Two Diabetes Mellitus

Type 2 diabetes mellitus (T2DM) is characterised by and preceded by a steady development of insulin resistance. Many molecular mechanisms have been explored with regards to the development of insulin resistance, and still there is no definitive mechanism by which insulin resistance occurs; it is likely a concerted combination of factors (Czech, 2017). A post receptor dysfunction of the PI-3 kinase, Akt pathway may cause downstream dysregulation of insulin mediated cellular processes. For instance, phosphorylation of IRS1 at serine 307, a post receptor dysfunction, reduces insulin signal transduction leading to insulin

resistance (Yaribeygi et al, 2018). Post receptor dysfunction is thought to be the major contributor to insulin resistance. However, it has been demonstrated that there is reduced presence of IR at the cell surface in obese and T2DM tissues, causing dysregulation of insulin mediated signalling pathways (Chen et al, 2019). Further to this, it has been demonstrated that diabetic plasma has increased levels of soluble IR compared to control subjects (American Diabetes Association, 2007). Additionally, Aβ concentrations have found to be elevated in T2DM and have been shown to perturb insulin signalling. Zhang et al (2012) demonstrated that hepatic insulin signalling was reduced via the upregulation of cytokine singling suppressors by Aβ.

A proteomic study identified the IR as a putative substrate for BACE1 and further predicted the sequence at which BACE1 would cleave IR (Johnson, Chambers and Jayasundera, 2013). Subsequently, it was established by Meakin et al (2018) that BACE1 cleaves the IR ectodomain in the liver. Here fragments of a peptide, including part of the predicted IR cleavage sequence, were detected using HPLC after cleavage by a soluble recombinant BACE1. Cleavage of IR would reduce cell surface concentrations of the IR and thus impact signalling as discussed above.

2.3.4. Vascular Pathology in T2DM

T2DM is itself considered a risk factor for both AD and VaD. In addition, all three conditions share numerous risk factors including high blood pressure, obesity, high cholesterol and smoking (Exalto et al, 2012). One major comorbidity of T2DM is the development of vascular complications leading to severe clinical outcomes such as diabetic retinopathy and the risk of limb amputation (Beckman and Creager, 2016). These and other diabetic clinical complications are mediated by upregulation or dysregulation of the angiogenic process in a tissue specific manor. Up regulation of angiogenesis in diabetic retinopathy, induced by ischemic conditions, propagates

the formation of new blood vessels which are prone to haemorrhage and potentially impair sight. However, impairment of collateral vessel formation in the diabetic state can lead to catastrophic patient outcomes including ischemic heart disease and cardiovascular disease. Across the spectrum of diabetic vascular complication, whether induced by upregulation or dysregulation of angiogenesis, there is a common theme of abnormal responses to hypoxia and proangiogenic factors such as VEGF (Fadini et al, 2019). Moreover, the increased levels of Aβ present in the plasma of T2DM patients, as discussed above, may impact on vascular health. In fact, Meakin et al (2020) demonstrated that obese mice were characterised by elevated levels of Aβ and EC dysfunction and that control mice infused with pathological concentrations of Aβ displayed vascular dysfunction.

2.4. Endothelial health

Endothelial cells (ECs) form the luminal layer of all vasculature throughout the body including in the brain where they form one of the 3 aspects of the blood brain barrier (BBB). Endothelial cells do not perform their function in the BBB alone they are one aspect of what is termed the neurovascular unit (NVU). Other cell types that make up the NVU are astrocytes, pericytes, neurons and microglia, all of which can modify the cerebrovascular response (McConnell et al, 2017). The other 2 aspects being the epithelial linings of the choroid plexus and the arachnoid. Functionally the BBB is responsible for maintaining the correct environment for neuronal function by regulation of the cerebral interstitial fluid via transport of substances such as ions across the BBB (Abbott et al, 2010). Maintenance of this environment is due to the specialisation of the ECs that line the brain vasculature. Specialisation occurs during embryonic development whereby BBB ECs develop a particular expression pattern in terms of transport proteins and tight junctions. Tight junctions are critical to integrity of the BBB as they prevent intercellular movement of neurotoxins form

the blood to the brain (Garlanda and Dejana, 1997). It has been demonstrated that the immediate environment of ECs induces tissue specific differentiation giving rise to functional characteristics. For instance, Janzer and Raff (1987) demonstrated that non brain ECs developed BBB characteristics when exposed to astrocytes in the anterior eye chamber of rats.

Endothelial dysfunction is concomitant with a wide range of vascular diseases and insulin resistant states. Delivery of oxygen and the correct nutrition for the proper function of all tissues in the body is provided by the body's vasculature, which is lined with ECs. Therefore, any EC dysfunction can have wide ranging pathophysiological effects (Endemann and Schiffrin, 2004) (Muniyappa and Sowers, 2014). In health the endothelium maintains a balance between opposing vasoactive factors including nitric oxide, which is a vasodilator and endothelin-1 (ET-1), a vasoconstrictor (Muniyappa and Sowers, 2014). Each of these is regulated by opposing branches of the insulin signalling cascade. The PI3-K, Akt branch mediates the stimulation of NO production via activation of eNOS (Figure 4). Alternatively, ET-1 upregulation is mediated via the MAPK branch of the cascade. Insulin resistant dependent endothelial dysfunction arises through the downregulation of the insulin, PI3-K, Akt signalling branch, whilst the MAPK branch is unaffected or upregulated, leading to an imbalance between NO and ET-1 (Rask-Madsen and King, 2007). Such an imbalance reduces the bioavailability of NO, which leads not only to reduced vasodilation but, increased inflammation and oxidative stress as NO is an inhibitor of inflammation and a quencher of reactive oxygen species (ROS) (Su, 2015). Inflammation and elevated levels of ROS induce ECs to express adhesion molecules that in turn promote migration of leukocytes into the sub-endothelial space. These mechanisms are implicated in the initiation of atherosclerosis (Zuliani et al, 2008). In fact, EC dysfunction has been postulated to be an initiating factor in a number of conditions. Separate studies of asymptomatic

subjects with a familial risk for T2DM, atherosclerosis and hypertension have displayed endothelial dysfunction (Endemann and Schiffrin, 2004). Additionally, the adhesion molecule VCAM-1, an indicator of endothelial dysfunction, appears in greater concentrations in the serum of those with AD and VaD, suggesting a role for endothelial dysfunction in the pathogenesis of these conditions (Zulinai et al, 2008). Furthermore, insulin resistance, also a characteristic of endothelial dysfunction, has been shown to increase the prevalence of biomarkers that typify AD (Hoscheidt et al, 2016). Together these observations point to a commonality between insulin resistance, endothelial dysfunction, and cognitive decline.

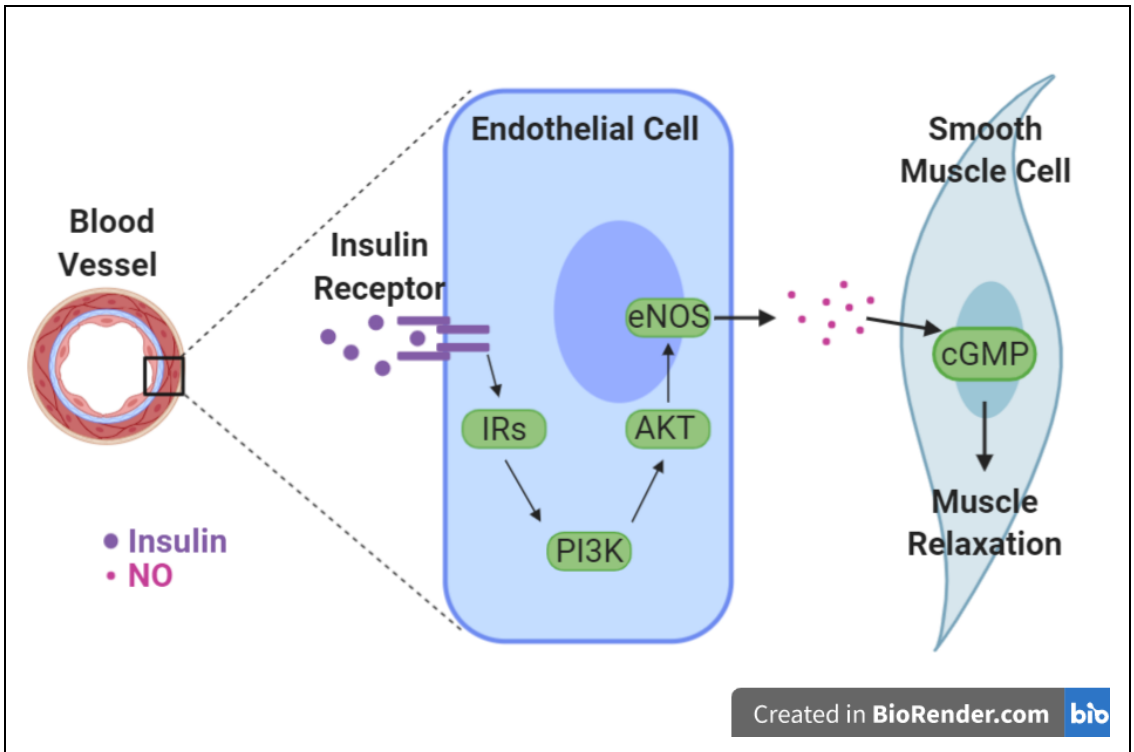

Figure 4: Insulin signalling in endothelial cells. Insulin binds its receptor at the surface of the luminal surface of the endothelial cell. Subsequently, a cascade of phosphorylation events occur that ultimately lead to the activation of eNOS and synthesis of nitric oxide (NO). Nitric oxide stimulates the vascular smooth muscle cells causing muscle relaxation and vasodilation, which induces improved perfusion.

3. Research problem statement

Vascular dementia is the second most prevalent form of dementia. The commonest form of dementia is AD and ~30% of cases display a vascular component. All dementias are characterised by cognitive decline and impediments on the patient's quality of life. At present there is no direct treatments for VaD, disease progression is managed via therapeutic or lifestyle interventions that target risk factors of VaD. Insulin resistance and T2DM have been closely associated with both vascular disease in the periphery and AD, although these links are poorly understood. BACE1 is already a target for drug development for the treatment of AD, with inhibitor drugs in various stages of clinical trials. BACE1 has recently been shown to cleave the insulin receptor, this could potentiate insulin resistance. Therefore, the current work seeks to bring understanding to the interplay between insulin mediated vascular effects and the modulation of BACE1 activity, with a view to providing insight into potential therapeutic targets for the treatment of VaD.

4. Hypothesis One

Inhibition or knockout of BACE1 will improve insulin stimulated Akt and eNOS signalling.

4.1. Objectives

1. Compare eNOS and Akt phosphorylation levels between BACE1 inhibited samples, BACE1 knockout samples and control samples when stimulated with insulin.
2. Compare the effects of BACE1 knockout or inhibition on eNOS and Akt phosphorylation levels between peripheral and brain endothelial cell lines stimulated with insulin.

3. Investigate the use of primary brain endothelial cells in the angiogenic bead assay.

5. Hypothesis Two

Inhibitors will interact differently with the BACE1 isoforms.

5.1. Objectives

1. Generate homology models of BACE1 isoforms
2. Carry out molecular docking simulations using BACE1 inhibitor C3

6. Hypothesis Three

BACE1 will show a greater affinity for APP than Insulin receptor.

6.1. Objective

1. Investigate differences in binding between APP and Insulin receptor to BACE1 using protein peptide docking simulations.

7. Materials and Methods

7.1. Experimental Procedures

7.1.1. Mice

All animal experimentation was carried out in accordance with the Animal and Scientific Procedures Act (1986). Mice were euthanised using CO_2.

7.1.2. Isolation of Murine Peripheral Endothelial Cells

Carried out by Jane Brown.

Murine lung pairs were minced using scalpels in a petri dish for approximately 10 minutes before being transferred to 15ml Falcon tubes with 10ml of 1mg/ml collagenase (Worthington's) solution, diluted in Hanks' Balanced Salt Solution (HBSS). Samples were incubated at 37^{o}C on a MacsMix rotator for 45 minutes. Samples were further homogenised using a 10ml stripette before being passed through a 70µm cell strainer and being rinsed with 8ml of cold Phosphate buffered saline (PBS). Samples were then centrifuged at 1200g at 5^{o}C for 5 minutes. Subsequently the pellet was aspirated, resuspended in 5ml PBS and the spin cycle was repeated. Samples were aspirated leaving 200µl of PBS and the pellet in situ, which was then transferred to an eppendorf tube. 20µl of CD146 mouse microbeads were added to the samples and gently mixed before being placed in a Miltenyi rotator and refrigerated for 20 minutes. Subsequently, samples were resuspended in 500µl of PBS and centrifuged at 4000g for 5 minutes. After centrifugation samples were resuspended in 500µl of a 1:15 dilution of Bovine Serum Albumin (BSA) solution in PBS before loading onto a cell separation column. Columns were washed with two lots of 1ml PBS-BSA mix, waiting until the first was fully eluted before adding the second. Subsequently, columns were placed over fresh Falcon tubes and 500µl of PBS-BSA mix was plunged through the column, eluting the PECs before centrifugation at 400g for 5 minutes. The pellet was aspirated before being resuspended in 6ml of warmed complete MV2 media (PromoCell). 1ml of the

cell suspension was aliquoted per well of a 6 well fibronectin coated plate and incubated for an hour and half. Spent media was aspirated and 1ml per well of fresh media was added before overnight incubation at 37^{o}C. Media was changed every other day until cells reached confluence. This procedure was conducted by Jane Brown.

7.1.3. Isolation of Murine Brain Endothelial Cells

Adapted from Bernard-Patrzynski (2019)

Murine brain tissue was minced using scalpels and was subsequently incubated at 37°C whist rotating for one hour in a 0.6 mg/ml solution of collagenase dispase (Roche) in Dulbecco's modified Eagle's medium – high glucose (Sigma-Aldrich) (DMEM). Digested tissue was further homogenised using a cannula in tandem with a 10 pipette and filler. Subsequently, homogenate was passed through a 70µL cell strainer and the resulting supernatant was centrifuged at 1000g for 10 minutes. Following this, the pellet was resuspended in a 20% BSA solution and centrifuged at 1000g for 20 minutes allowing the separation of the myelin. Myelin was removed via aspiration and the pellet resuspended in 5 ml of phosphate-buffer saline (PBS) before centrifugation at 400g for 5 minutes. Supernatant was aspirated and the pellet resuspended in complete MV2 endothelial growth media (PromoCell) before seeding into either a 6 well plate or T75 flask. Cells were maintained at 37°C, 5% CO_2.

7.1.4. Mammalian Cell Culture

Murine primary brain endothelial cells were maintained in complete MV2 endothelial media. A complete media change was carried out every over day till cells reached confluence. Typically, cells reached confluence at one week of incubation and were stimulated and treated at this point, they were not passaged. Upon reaching

confluence both PECs and BECs were visualised under a light microscope to observe their morphology to establish that the cell line was endothelial and free from contamination. Additionally, PECs were passed through columns containing CD146 microbeads (as described in 7.1.1.), a commonly used endothelial marker, to sort endothelial cells from other cell types present in the homogenate.

7.1.5. Cell Culture Stimulation and Harvest

These experiments were subject to biological replicates only as the yield of cells isolated from one mouse brain was insufficient to carry out technical replicates too. Confluent primary cells in the 6 well plates were serum starved in 0.1% FBS MV2 media. The C3 BACE-1 inhibitor, purchased from Merk (Nottingham, UK), was also applied at this stage at a concentration of 250nM dissolved in DMSO, with untreated samples receiving a concentration matched DMSO only dose. Samples were subsequently incubated at 37°C for 24 hours. After 24 hours samples were stimulated with 10nM and 100nM of human insulin (Sigma-Aldrich: cat. No.19278) diluted in MV2 endothelial growth media and left to incubate for 15 minutes. Insulin concentrations were selected to elicit measurable effects on the downstream signalling molecules (Akt and eNOS). 100µl of Cell extraction buffer (ThermoFisher: FNN0011), with 1µl/ml of both phosphatase and protease inhibitors added, per well was used to lyse the cells. Samples were then scraped, collected in eppendorf tubes, and stored at -20°C till further use.

7.1.6. Protein Quantification Assay

Using the Pierce BCA assay kit (cat. no. 23227) protein content of the cell lysates was measured. First, standards ranging in concentration from 0 to 2000 µl/ml were prepared. In order to prepare the samples for quantification they were first diluted by adding 52.5µl of water to 7.5µl of the sample. Diluted samples and standards were then added to a ninety-six well plate, in duplicate. The reaction reagents were then

added to all wells before incubation of the plate at 37°C for half an hour. Plates were read at 562nm. Results were analysed using excel.

7.1.7. Western Blot

Table 1: Primary anti body details

Antibody	Supplier	Cat. no.	Host species	Dilution
Anti AKT	Cell Signalling	9272s	Rabbit	1 in 1000
Anti eNOS	BD Biosciences	610297	Mouse	1 in 2000 - 3000
Anti-phosphorylated AKT$^{(Ser473)}$	Cell Signalling	4060s	Rabbit	1 in 2000
Anti-phosphorylated eNOS$^{(Ser1177)}$	Cell Signalling	9571s	Rabbit	1 in 1000
Beta actin	Santa Cruz	SC-47778	Mouse	1 in 2500 - 3000

Table 2: Secondary antibody details

Antibody	Supplier	Cat. no.	Dilution
Mouse	Cytiva	ECL NA931V	1µl in 5000µl
Rabbit	Cytiva	ECL NA934V	1µl in 5000µl

10µg of protein was suspended in 20µl or 35µl, samples were then loaded onto 15 and 10 well gels respectively. Gels were then run at 110V for 2 hours and 20 minutes. Subsequently, the gel was transferred to a transfer membrane using a wet transfer method at 100V for 1 hour. The membrane was cut at around 100KDa and placed in a 5% BSA, TBS, 0.01% tween blocking buffer for half an hour on a rocker at RT. Primary antibodies were diluted with 5% BSA, TBS, 0.01% tween blocking buffer, applied to the corresponding membrane and left on overnight at 4°C on a rocker. Following this the membranes were washed, and the secondary antibodies applied and left to react at RT on a rocker for 1 hour before the development of the

membranes using ECL immobilon. Images were captured using GENESYS software and saved as tiff files.

7.1.8. Western Blot Analysis

Tiff files were opened in Image J (Schneider, Rasband and Eliceiri, 2012) and the intensity of the bands were measured and exported into Excel. In Excel band intensities of the target protein was normalised to the according band intensity of Beta Actin, from the same gel and lane. Furthermore, target protein band intensities were normalised to the band intensity of the control sample of the same sample group.

7.1.9. Angiogenic Bead Assay

Adapted from Nakatsu, Davis and Hughes (2007)

Confluent primary murine brain endothelial cells (BECs) were trypsinised and 8ml of MV2 was added to neutralise the reaction before transferring the cells to a 15ml falcon tube using a pipette. Subsequently, cells were centrifuged for five minutes at 500g before aspiration of the MV2. Cells were agitated and resuspended in 4ml of MV2 before cell counting. 10µl of both cell suspension and trypan blue were placed in an eppendorf, 10µl of the mixture was pipetted onto a haemocytometer, cells were counted, and a cell concentration calculated.

21µl of Cytodex bead suspension, per condition, was aliquoted into clean eppendorf tubes with 50µl of PBS. Beads were left to settle for five minutes before aspirating the supernatant, leaving the beads at the bottom of the tube. Beads were resuspended in 1ml MV2, left to settle and supernatant was aspirated before the addition of 1ml of the cell suspension. Subsequently the cell, bead suspensions were transferred to FACS tubes and incubated for four hours; tubes were agitated every twenty minutes during this period. After incubation the contents of the FACS tubes are transferred to T25 flasks and 4ml of MV2 added before incubating

overnight at 37^{o}C. Cell, bead suspension was aspirated, resuspended in 1ml of MV2 and transferred to 1.5ml eppendorf's before leaving to settle for five minutes.
The cell, bead suspensions were transferred from T25 flasks to 15ml falcon tubes, flasks were rinsed with two 2ml aliquots of MV2 and left to settle for fifteen minutes.
Fibrinogen was prepared using 2mg/ml of warm PBS and filter sterilised.
Suspensions were subsequently washed three times using a 1ml aliquots of MV2 each time before resuspension in 2.5ml of the prepared fibrinogen.
12.5µl of thrombin was pipetted into each well of a 24 well plate. Subsequently, 500µl of the cell, bead, fibrinogen suspension was gently added to each well ensuring a good distribution of beads within the thrombin clots. Samples were incubated at 37^{o}C for fifteen minutes allowing clots to solidify. 1ml of MV2 was added to each well before samples were incubated for twenty-four hours before imaging.

7.1.10. Angiogenic Bead Assay Image Analysis

Beads were imaged individually and analysed using Image J software, in which a scale was set. Sprout length and quantity was recorded for each bead. Seven beads per well and four well per condition were analysed (Schneider, Rasband and Eliceiri, 2012).

7.1.11. Statistical and data Analysis

Excel was used to generate normalised values for data gathered from western blot and bead assay experiments. Data was then exported to Graph Pad in order to graph the results obtained. Western blot data was subject to a two-way ANOVA and multiple comparison tests in GraphPad Prism version 8.4.3 for windows, GraphPad Software, San Diego, California USA, www.graphpad.com.

7.2. Computational Methods

7.2.1. Building homology models

Adapted from Waterhouse et al (2018)

FASTA sequences of all six BACE1 isoforms were retrieved from the Uniprot database. Subsequently, using the National Centre for Biotechnology Information (NCBI) protein BLAST tool the FASTA sequences were aligned against structures deposited in the Protein Data Bank (PDB) in order to select an appropriate template structure on which to build the homology models (Altschul et al, 1990). The structure displaying the greatest query coverage was assessed for its quality by checking for outliers in its Ramachandran plot before being selected as the appropriate template. Preparation of the template was done using PyMol, where water and the co-crystallised ligand was removed (DeLano, 2002). The prepared template and FASTA sequences were input to the SWISS-MODEL server to produce homology models of the six BACE1 isoforms. Quality of the homology models were assessed using the global quality estimates generated by SWISS-MODEL and alignment of the model with the template structure in PyMol where the RMSD value was considered. Models were saved in PDB format.

7.2.2. Validation of docking procedure

Adapted from AutoDock Vina tutorial (Trott and Olson, 2010).

A homology-model of BACE1-A was created and docked with the conjugate ligand of the template structure. The PDB structure of the template was opened in PyMol along with the most favourable pose generated by AutoDock Vina. These two structures were aligned and the orientation of the docked ligand from the experiment was compared with that of the co-crystallised ligand.

7.2.3. Docking of C3

The structure of C3 was downloaded in PDB format from the PDBe database. Using BIOVIA Discovery Studio polar hydrogens were added to the BACE1 isoform homology-models. The template structure, including the co-crystallised ligand was used to define a binding region in BIOVIA Discovery Studio. In AutoDock Vina PDB files of both the prepared homology-models and the C3 ligand were converted to PDBQT format. The binding region coordinates, receptor and ligand PDBQT files were input into AutoDock Vina yielding eight predicted docking poses for each homology-model.

7.2.4. Docking of oligopeptides for APP and IR

Adapted from Zhou et al (2018).

An eight amino acid binding motif of both APP and IR was composed in PDB format using PyMol. These oligopeptides were then docked, using the HPEPDOCK server, with homology models of each BACE1 isoform prepared as previously described (7.2.1). The blind docking parameters were used.

7.2.5. Analysis of docking results

Using the log file output generated by AutoDock Vina the pose with the best affinity score was selected for each isoform model docked with the C3 inhibitor. In the case of the peptide docking simulations the docking score and cluster size generated by HPEPDOCK was used to determine the best pose for each model. Opening the docking results in BIOVIA Discovery Studio allowed receptor-ligand interactions to be examined and visualised, collecting data on contact residues and types of bonds present in the complex (BIOVIA, 2020).

8. Results

8.1. Experimental procedures

8.1.1. Insulin mediated Akt and eNOS signalling in wild type and BACE-1$^{-/-}$ PECs

To investigate a link between BACE1 activity and insulin mediated endothelial function peripheral ECs were isolated from lung tissues of wild type and BACE1$^{-/-}$ mice and subsequently stimulated with 0nM, 10nM and 100nM concentrations of insulin. Protein was harvested and quantified before analysis by western blot to observe levels of Akt and eNOS activity.

When examined for the effects of the BACE1$^{-/-}$ genotype on insulin mediated total Akt signalling there was found to be no statistical significance to the results (Figure 5, B). This is demonstrated by the difference in the sample means, at a confidence interval (CI) of 95%, of -1.352 to 0.03149; a mean difference spanning zero indicates no significance in total Akt signalling between genotypes. Meaning the genotype has not significantly affected expression levels of total Akt.

However, the effect on total Akt signal intensity provided by the BACE1 deficient genotype displays a P value of 0.0597. Additionaly, the difference in genoype accounts for the majority of the varience in Akt signaling; contributing 25.71% compared to 2.565 and 0.4008 % demonstrated by insulin-genotype interaction and insulin stimulation respectivley. Whilst this is currently not significant it may be improved by adding to the n number, as the current N of 3 is to low to provide a clear picture.

Quantification of phosphorylated Akt (P-Akt) revealed an observable pattern of increased P-Akt signaling in the BACE1$^{-/-}$ genotype paired with a dose dependent

signaling increase in the presence of insulin (Figure 5, C). Furthermore, genotype was responsible for a significant proportion of the variation in the result (11.40%) with a P-value of 0.0020 (**). Significance of the signalling difference between genotypes is further demonstrated by the 95% CI of difference of -0.8636 to -0.2056, which does not span zero meaning the contribution of the genotype to signaling is significant. However, it was insulin stimulation that demonstrated the largest contribution to variation at 37.72% with a P-value of <0.0001 (****). Interaction between genotype and insulin stimulation provided no significant source of variation, indicating increased phosphorylation of Akt observed in the BACE1$^{-/-}$ genotype was occuring at the basal level and independent of insulin action.

Ratios of phosphorylated to total Akt proteins, in wild type and BACE1$^{-/-}$ samples, suggests a blunting of signal transduction in BACE1$^{-/-}$ ECs (Figure 5, D). Here, insulin made the only significant contribution to variation at 35.11% with a P-value of 0.0454 (*). Genotype makes no significant contribution to signalling based on a 95% CI of difference of -0.2046 to 1.36 and a source of variation value of 11.24% with a P-value of 0.1335.

However, large standard error of the mean (SEM) values across the data sets may be reduced with an increase in the sample size. In turn the contribution of the BACE1$^{-/-}$ genotype to signal transduction will become clearer.

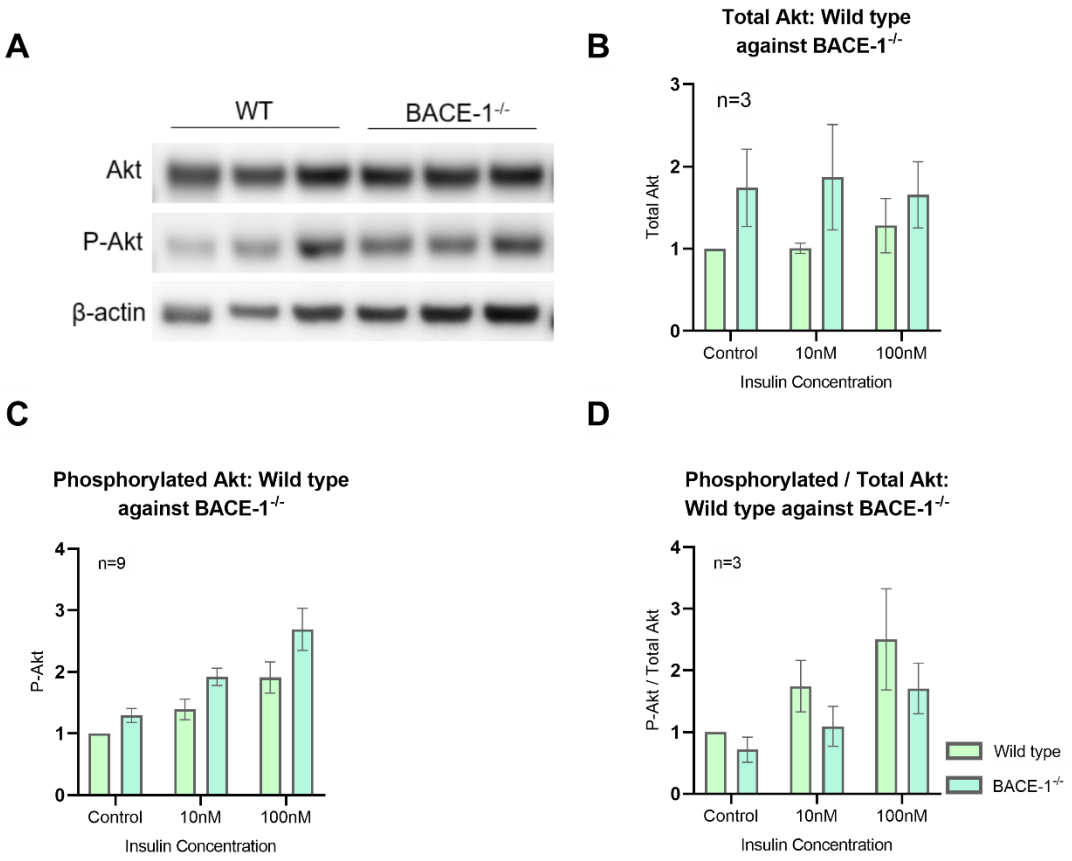

Figure 5: Insulin mediated Akt signalling in wild type and BACE-1$^{-/-}$ PECS. (**A**) Representative image of western blot of total Akt, Phosphorylated Akt$^{(Ser473)}$ and β-actin in PECs from wild type and BACE-1$^{-/-}$ mice when stimulated with insulin. (**B**) Signal induced by Akt in PECs from wild type and BACE-1$^{-/-}$ mice when stimulated with insulin. (**C**) Signal induced by Phosphrylated Akt$^{(Ser473)}$ in PECs from wild type and BACE-1$^{-/-}$ mice when stimulated with insulin. (**D**) Signal ratio of Phosphorylated Akt to Akt in PECs from wild type and BACE-1$^{-/-}$ mice when stimulated with insulin. Data presented is mean ± standard error of the mean. Data was analysed using 2 way ANOVA and Tukey tests.

Insulin treatment did not induce a significant change in total eNOS expression (Figure 6, B). Large variations of the SEM in the BACE1$^{-/-}$ data sets will have a probable impact on this lack of significance and may be remedied by an increase in sample size. However, genotype is the greatest contributing factor in the variance of

total eNOS signal intensities at 60.17% with a P-value of 0.0009 (***). Suggesting the absence of the BACE1 gene could effect expression levels of eNOS.

Differences in phosphorylated eNOS (P-eNOS) are significantly affected by both insulin stimulation and genotype (Figure 6, C) with insulin stimulation being the greatest source of variation at 17.10% with a P-value of 0.0203 (*). The level of contribution to variation provided by genotype is also significant at 10.36% with a P-value of 0.0276 (*). In addition to this the 95% CI of differnce of -1.073 to -0.06668 does not span zero and therefore demonstrates the significance of the genotypic contribution to P-eNOS signalling. Results indicate BACE1 knockout increases eNOS activation via elevated phosphorylation of eNOS, observed in the BACE1 knockout ECs. Such elevations occur in both insulin stimulated and control ECs, suggesting increased P-eNOS present in the $BACE1^{-/-}$ genotype may be independent of insulin stimulation.

Phosphorylated-total ratios of eNOS signal intensities appear to show a blunting of signaling in the $BACE1^{-/-}$ genotype (Figure 6, D). It should be noted that the sample size here is low, therefore a solid conclusion on the signaling pattern can not be drawn. However, the differences in signaling are mainly a function of genotype with a contribution of 43.81% and a P-value of 0.0066 (**).

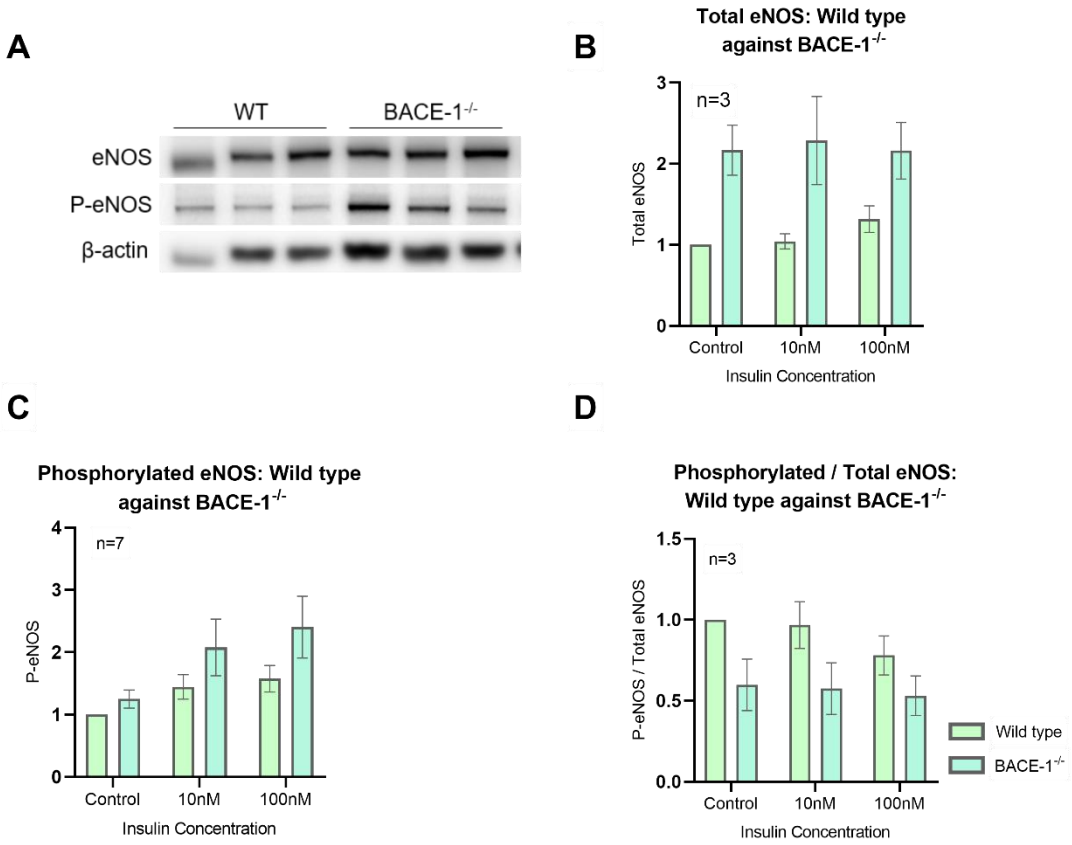

Figure 6: Insulin mediated eNOS signalling in wild type and BACE-1$^{-/-}$ PECS. (**A**) Representative image of western blot of total eNOS, Phosphorylated eNOS$^{(Ser1177)}$ and β-actin in PECs from wild type and BACE-1$^{-/-}$ mice when stimulated with insulin. (**B**) Signal induced by eNOS in PECs from wild type and BACE-1$^{-/-}$ mice when stimulated with insulin. (**C**) Signal induced by Phosphrylated eNOS$^{(Ser1177)}$ in PECs from wild type and BACE-1$^{-/-}$ mice when stimulated with insulin. (**D**) Signal ratio of Phosphorylated eNOS to eNOS in PECs from wild type and BACE-1$^{-/-}$ mice when stimulated with insulin. Data presented is mean ± standard error of the mean. Data was analysed using 2 way ANOVA and Tukey tests.

8.1.2. Insulin mediated Akt and eNOS signalling in wild type and inhibitor (C3) treated PECs

We have established that genetic knockout of the BACE1 gene increases phosphorylation of both Akt and eNOS in peripheral endothelial cells. Next, we

wanted to determine if pharmacological inhibition of BACE1 would carry the same effect.

Peripheral ECs were isolated from lung tissues of wild type mice and were subsequently seeded into six conditions. The BACE1 inhibitor C3 was prepared in DMSO and applied to three of the six conditions, with the other three conditions receiving a DMSO vehicle control. After twenty-four hours incubation cells in both control and C3 treated conditions were stimulated with 0nM, 10nM and 100nM concentrations of insulin. Protein was extracted from the lysates and quantified before analysis by western blot.

Analysis of total Akt signaling reveals there is no significant difference between C3 treated and untreated ECs demonstrated by the 95% CI of difference of -0.4456 to 0.1546 (Figure 7, B).

Measurment of P-Akt reveals a significant difference in signal intensity between treated and untreated ECs at an insulin concentration of 100nM with a P-value of 0.0396 (*) (Figure 7, C). Furthermore, the 95% CI of difference is -1.551 to -0.1945, which does not span zero thus demonstarting the difference between treated and untreated ECs is significant. Although, it should be noted that the major contributor to signaling difference in this data set is insulin accounting for 25.61% of the variation with a P-value of <0.0001 (****). Here, results demonstrate the ability of BACE1 inhibition to increase the phosphorylation of Akt.

Ratios of phosphorylated and total Akt proteins display no significant difference in signaling between treated and untreated ECs; this is demonstrated by the 95% CI of differnec of -0.5412 to 0.8460 (Figure 7, D). In fact, insulin accounts for 29.46% (P-value 0.0002) of the sampe variation and is the largest contributor to variation.

Again, ratios of signal intensities appear to demonstrate a dampening of signal transduction in the ECs treated with C3.

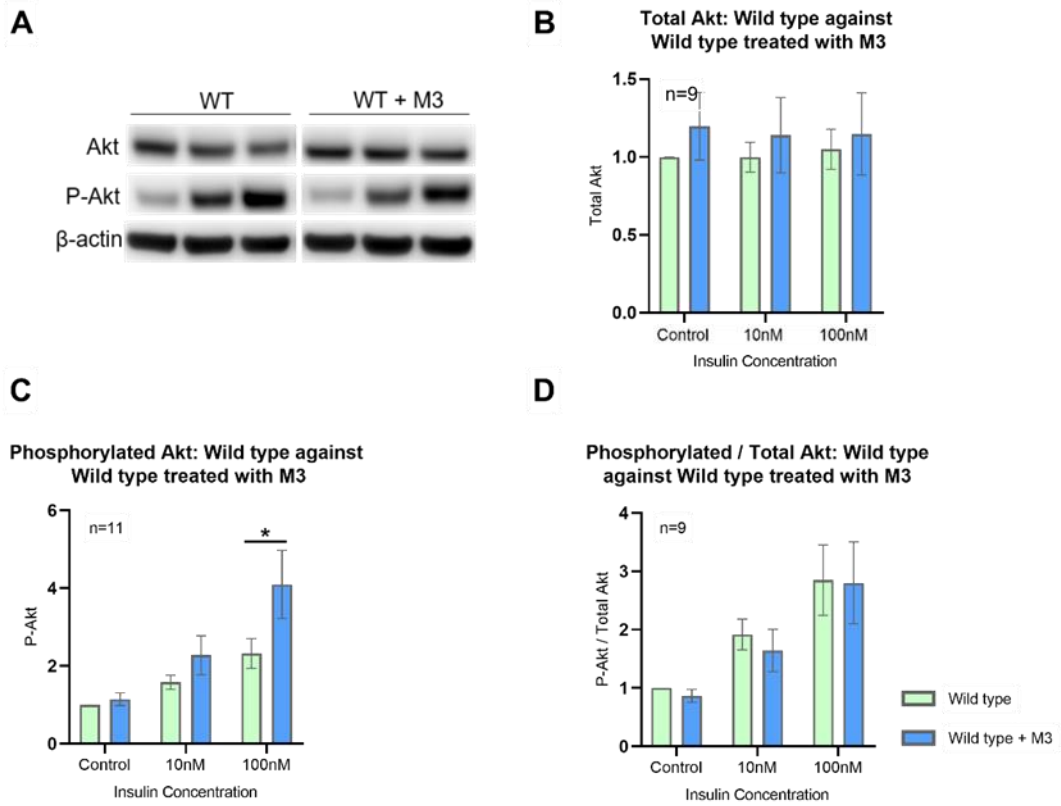

Figure 7: Insulin mediated Akt signalling in wild type and wild type treated with C3 PECS. (**A**) Representative image of western blot of total Akt, Phosphorylated Akt$^{(Ser473)}$ and β-actin from wild type and wild type treated with BACE-1 inhibitor (C3) murine PECs. (**B**) Signal induced by Akt in wild type and wild type treated with BACE-1 inhibitor (C3) murine PECs when stimulated with insulin. (**C**) Signal induced by Phosphrylated Akt$^{(Ser473)}$ in wild type and wild type treated with BACE-1 inhibitor. (C3) murine PECs when stimulated with insulin. (**D**) Signal ratio of Phosphorylated Akt to Akt in wild type and wild type treated with BACE-1 inhibitor (C3) murine PECs when stimulated with insulin. Data presented is mean ± standard error of the mean. Data was analysed using 2 way ANOVA and Tukey tests. *$p < 0.05$

Signal intensites as a measure of total eNOS demonstrate no significance difference between C3 treated and untreated ECs with a 95% CI of difference of -0.9479 to 0.1837, these values span zero indicating no significance between sample C3 treated and untreated groups (Figure 8, B).

Endothelial cells under control conditions exhibit a significant differnce in P-eNOS signal intensities between C3 treated and untreated ECs, with a P-value of 0.0244, with C3 treated ECs showing elevated levels of P-eNOS (Figure 8, C). The contribution of BACE1 inhibition to the overall varience is 20.67% with a P-value of 0.0001; it is the largest contributing factor. Moreover, values of the 95% CI of difference that do not span zero (-0.5649 to -0.1992) also demonstrate the significance in signaling difference between the treated and untreated ECs.

In contrast to figures 5, 6 and 7 the ratios of phosphorylated-total eNOS appear to show an observable trend of increased signal intensity in C3 treated ECs (Figure 8, D). However, there is no significant differance in signal intensites between treated and untreated ECs. The 95% CI of differnce of -0.6194 to 0.2873 spans zero and demonstrates the lack of signifcant difference between the C3 treated and untreated samples in terms of phosphorylated-total eNOS ratios.

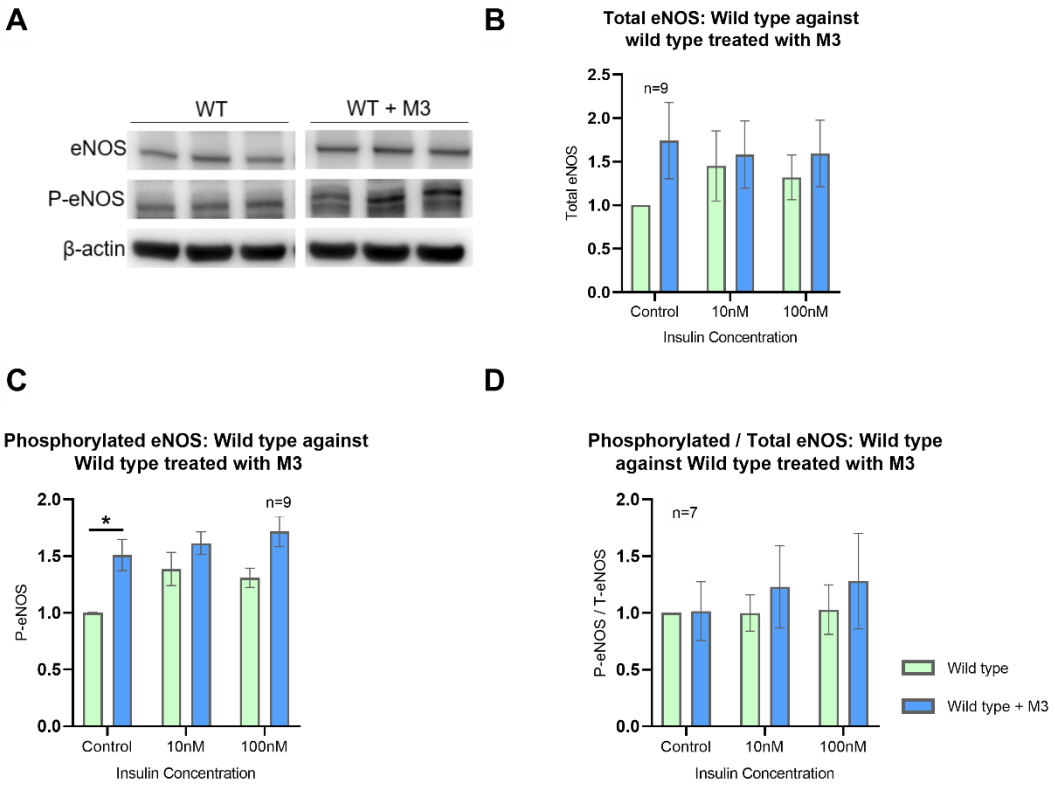

Figure 8: Insulin mediated eNOS signalling in wild type and wild type treated with C3 PECS. (**A**) Representative image of western blot of total eNOS, Phosphorylated eNOS$^{(Ser1177)}$ and β-actin from wild type and wild type treated with BACE-1 inhibitor (C3) murine PECs. (**B**) Signal induced by eNOS in wild type and wild type treated with BACE-1 inhibitor (C3) murine PECs when stimulated with insulin. (**C**) Signal induced by Phosphrylated eNOS$^{(Ser1177)}$ in wild type and wild type treated with BACE-1 inhibitor (C3) murine PECs when stimulated with insulin. (**D**) Signal ratio of Phosphorylated eNOS to eNOS in wild type and wild type treated with BACE-1 inhibitor (C3) murine PECs when stimulated with insulin. Data presented is mean ± standard error of the mean. Data was analysed using 2 way ANOVA and Tukey tests. *$p < 0.05$

8.1.3. Insulin mediated Akt and eNOS signalling in wild type and BACE-1$^{-/-}$ BECs

Having established a pattern of increased Akt and eNOS phosphorylation in BACE1 pharmacologically and genetically inhibited peripheral endothelial we moved to establish if these patterns would be present in brain derived endothelial cells.

Endothelial cells were isolated from wild type and BACE1$^{-/-}$ murine brains. Cells were subsequently exposed to a 0nM, 10nM or 100nM of insulin before being harvested. Protein content was quantified using the BCA assay before undergoing analysis via western blotting.

Analysis of total, phosphorylated and their ratio of Akt signal intensities of wild type and BACE1$^{-/-}$ samples demonstrate some relatively large SEMs, particularly in the BACE1$^{-/-}$ samples (Figure 9). Such margins of error may be reduced by increasing the sample size.

In the case of total Akt signal intensities, genotype makes a significant contribution to variation in the samples of 32.91% with a P-value of 0.0040 (Figure 9, B). Furthermore, the 95% CI of 0.1371 to 0.6193 does not span zero indicating the significant contribution of genotype to sample differences. However, there is no such significant difference in signalling between the genotypes in measurements of P-Akt and the phosphorylated-total ratios (Figure 9, C and D). Both phosphorylated and ratio signal intensities have 95% CI of difference values that span zero (-0.2320 to 0.7067 and -1.218 to 0.2879 respectivly) demonstrating this absence of significance.

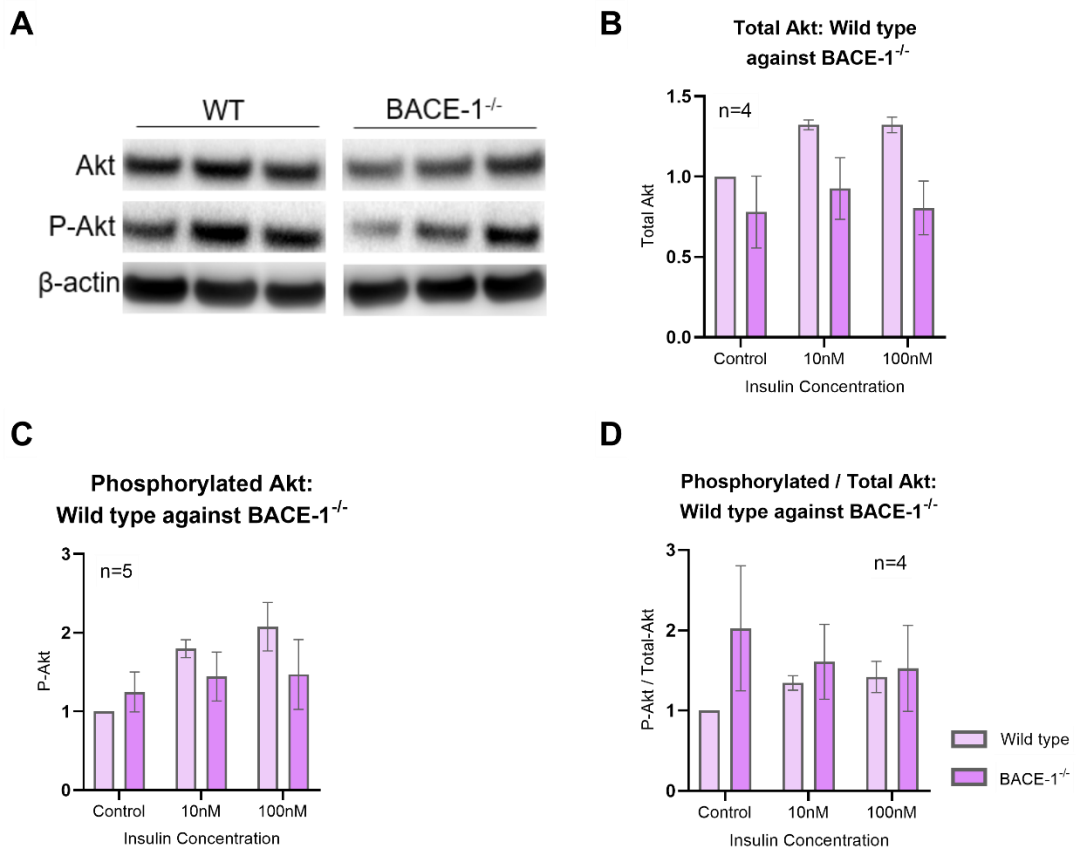

Figure 9: Insulin mediated Akt signalling in wild type and BACE-1$^{-/-}$ BECS. (**A**) Representative image of western blot of total Akt, Phosphorylated Akt$^{(Ser473)}$ and β-actin in BECs from wild type and BACE-1$^{-/-}$ mice when stimulated with insulin. (**B**) Signal induced by Akt in BECs from wild type and BACE-1$^{-/-}$ mice when stimulated with insulin. (**C**) Signal induced by Phosphrylated Akt$^{(Ser473)}$ in BECs from wild type and BACE-1$^{-/-}$ mice when stimulated with insulin. (**D**) Signal ratio of Phosphorylated Akt to Akt in BECs from wild type and BACE-1$^{-/-}$ mice when stimulated with insulin. Data presented is mean ± standard error of the mean. Data was analysed using 2 way ANOVA and Tukey tests.

Measurement of eNOS signaling in wild type and BACE1$^{-/-}$ BECs (Figure 10) display relatively large SEM bars on the BACE1$^{-/-}$ samples. Here, the sample size is low and it is likely that the SEM would reduce with increased sample numbers. Measures of total eNOS are the only results where the genotype has significantly contributed to the variation between genotypes, with a contribution of 21.39% and a P-value of

0.0169 (*). Also, total eNOS signal intensities exhibit a 95% CI of difference of 0.05525 to 0.5075, further demonstrating the significant contribution of genotype to signaling differences. Signal intensites recordered for phosphorylated and phosphorylated-total ratios of eNOS do not display any significant difference in signaling between genotypes, with 95% CI of differences of -0.9663 to 0.1195 and -1.433 to 0.1692 respectivly. Results demonstrate the potential for BACE1 inhibition to increase expression levels of eNOS.

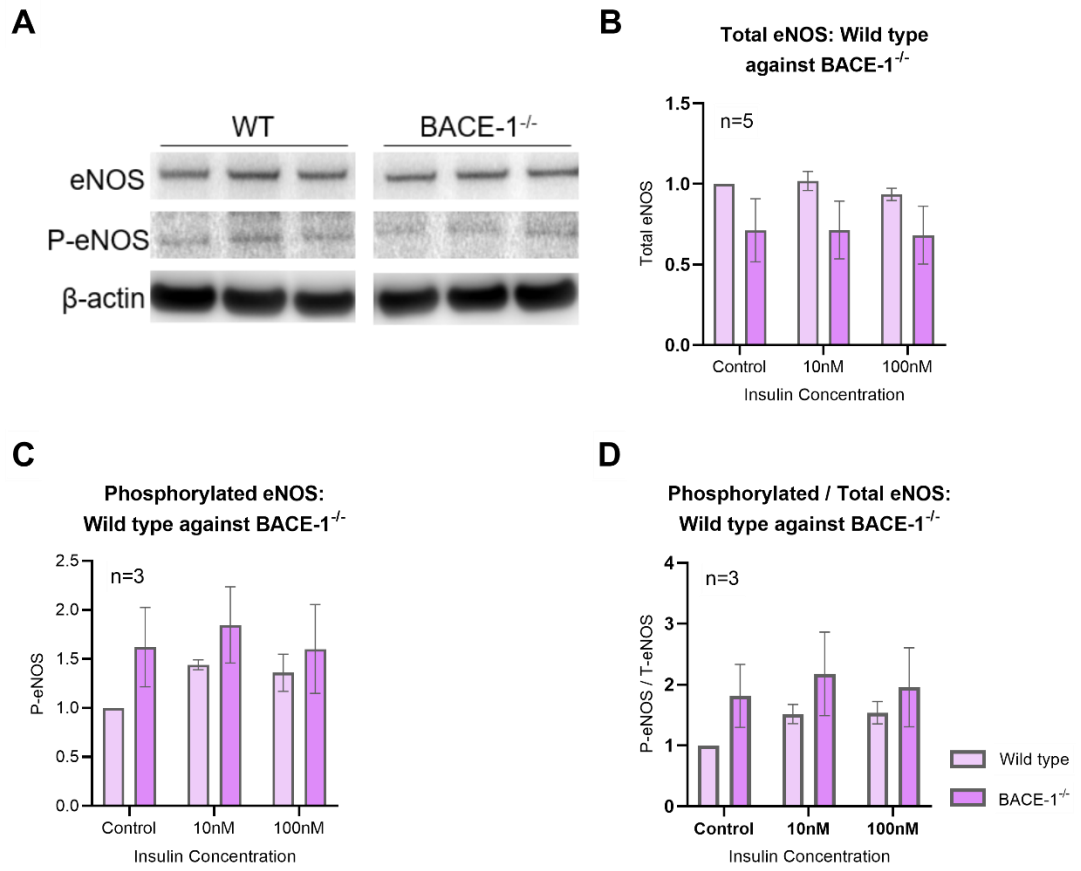

Figure 10: Insulin mediated eNOS signalling in wild type and BACE-1$^{-/-}$ BECS. (**A**) Representative image of western blot of total eNOS, Phosphorylated eNOS$^{(Ser1177)}$ and β-actin in BECs from wild type and BACE-1$^{-/-}$ mice when stimulated with insulin. (**B**) Signal induced by eNOS in BECs from wild type and BACE-1$^{-/-}$ mice when stimulated with insulin. (**C**) Signal induced by Phosphrylated eNOS$^{(Ser1177)}$ in BECs from wild type and BACE-1$^{-/-}$ mice when stimulated with insulin. (**D**) Signal ratio of Phosphorylated eNOS to eNOS in BECs from wild type and BACE-1$^{-/-}$ mice when stimulated with insulin. Data presented is mean ± standard error of the mean. Data was analysed using 2 way ANOVA and Tukey tests.

8.1.4. BEC's Angiogenic bead assay pilot

As the peripheral ECs demonstrated increased Akt and eNOS phosphorylation and with data from BECs showing potential to follow suit we wanted to investigate the functional implications of the changes in expression of Akt and eNOS. To do this we

used the angiogenic bead sprouting assay. However, we did this using ECs isolated from brain tissue, which according to current literature does not appear to have been tried before.

Endothelial cells were isolated from wild type murine brain tissues, were incubated and allowed to reach confluence before being used to perform the angiogenic bead assay under control conditions. Four wells were used in this pilot to assess the viability of using primary BECs in this assay. Results were analysed with Image J software and GraphPad.

Results demonstrate that primary BECs are viable for use in the angiogenic bead assay (Figure 11). With largely consistent results for both sprout number and sprout length across the four wells.

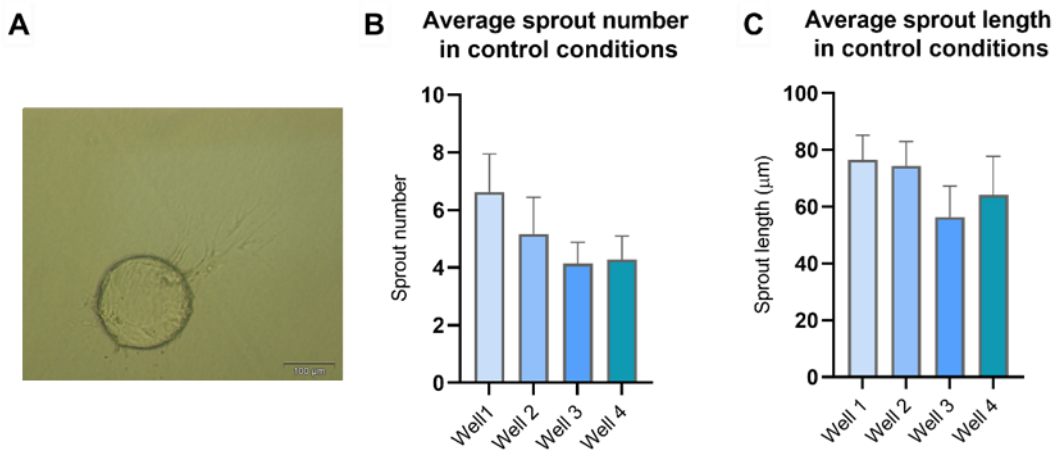

Figure 11: Angiogenic bead assay in control conditions using BECs.
(**A**) Representative image of a bead coated with BECs in control conditions. (**B**) Average number of sprouts per bead in each well under control conditions. (**C**) Average sprout length (µm) under control conditions.

8.2. Computational simulations

8.2.1. Docking of BACE1 inhibitor C3 in BACE1 isoform homology models

There are six known BACE1 isoforms, A, B, C, D, 5 and 6. Currently only the crystal structure of isoform A has been solved. Models of BACE1 isoforms were constructed using a BACE1 crystal structure as a template. For isoform A the empty template structure was used in the docking experiments. Models were assessed for their quality before using AutoDock Vina in the docking of the BACE1 inhibitor C3. Analysis of docking outcomes was done using Discovery studio and PyMol.

All homology models produced display good levels of quality. Interpretation of the root mean square deviation (RMSD) depends upon the resolution of the template structure. Here, the template structure (6EJ3 in the PDB) was solved by X-ray diffraction and has a resolution of 1.94Å. Therefore, a RMSD of <1.94 would be considered good; all isoform models display a RMSD lower than this (Table 3) with

values ranging from 0.21 to 1.26. Furthermore, the TM-align tool was used to help assess model quality; this algorithm analyses the alignment of two protein structures to generate a TM-score between 0 and 1, where 1 indicates perfect alignment (Zhang and Skolnick, 2005). All models exhibit a TM-score close to 1 with ranging from 0.81445 to 0.95765 (Table 3). Models were constructed using SWISS-MODEL which also generates quality assessment data for the model template alignment. In particular the QMEAN score, a descriptor of the degree of nativeness of a model, should not fall below -4.0 as this indicates the model is of low quality. All isoform models have values above -4.0, ranging from -0.06 to -1.22 (Table 3) (Figure 12). Taken together these data suggest the BACE1 isoform models constructed are of a high quality.

In addition to the data driven quality assessments, models were visualised in PyMol. Figure 12, C shows the template and BACE1-B model aligned; it can be seen that the structures closely match. Furthermore, upon alignment of the template and model measurement were taken of distances between the model and template key BACE1 residues, D32 and D228 (Figure 12, D). Measurements range from 0.1 to 0.6 Å, which again demonstrates the close alignment of model and template.

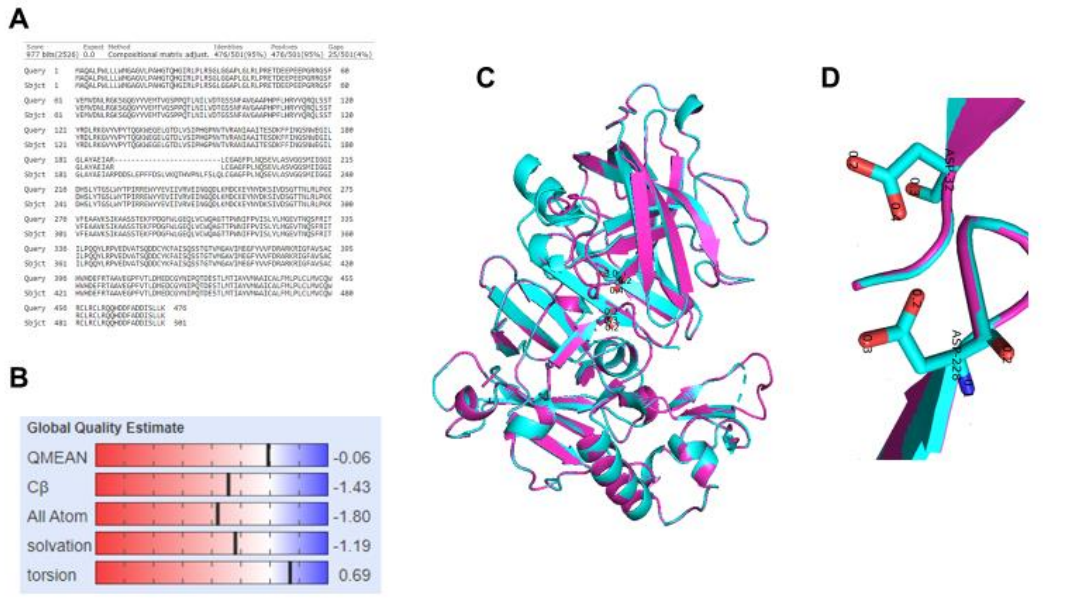

Figure 12: Building and validation of homology-models. (A) Sequence alignment between query sequence (BACE1 isoform) and that of crystal structure with greatest query coverage (6EJ3). **(B)** Global quality scores for homology model generated using query sequence and template structure (6EJ3) in SWISS-MODEL. **(C)** Visual alignment of template and model constructed in PyMol; blue and magenta represent the template and model respectively. **(D)** Close-up view of key active site residues in the aligned template and model.

Table 3: RMSD values of BACE1 isoform homology models aligned to the template structure (6EJ3)

BACE1 Isoform	RMSD	TM-score	QMEAN
B	0.71	0.95765	-0.06
C	0.79	0.87520	-0.55
D	1.26	0.81445	-0.71
5	0.21	0.88786	-1.12
6	0.60	0.85126	-1.22

In PyMol the key catalytic BACE1 residues were identified in the template structure. Model and template were aligned and the numbering of the key residues in the models were derived (Table 4).

Table 4: BACE1 key binding residue alignments

BACE1 isoform	**Key BACE1 binding residues**		
BACE1-A	**D32**	**Y71**	**D228**
BACE1-B	D93	Y132	D264
BACE1-C	D93	Y132	D245
BACE1-D	D93	Y132	D220
BACE1-5	Missing	Y32	D189
BACE1-6	Missing	Y32	D164

BACE1 Crystal structure 6EJ3, from PDB, was used as a template for the construction of all homology models in the current work. This structure was co-crystallised with the inhibitor B7T. To test the prediction capabilities of the docking software (AutoDock Vina) B7T was docked with an empty template. Visualisation of the docking results show the eight poses generated appear in varying orientations within the BACE1 binding pocket (Figure 13, A and B). The most energetically favourable predicted binding pose was then aligned with the pose captured in the co-crystallised structure (Figure 13, C). The predicted pose is orientated in the same plane as the co-crystallised structure. The close alignment of the docked B7T inhibitor with the co-crystalised structure indicates the AutoDock software's ability to accurately predict binding poses of ligands within receptor active sites. However, due to several rotating bonds present in the B7T molecule, the terminal aromatic ring of the predicted pose is rotated away from the co-crystallised structure at an angle of 151^{O} indicating some inaccuracies in the docking software.

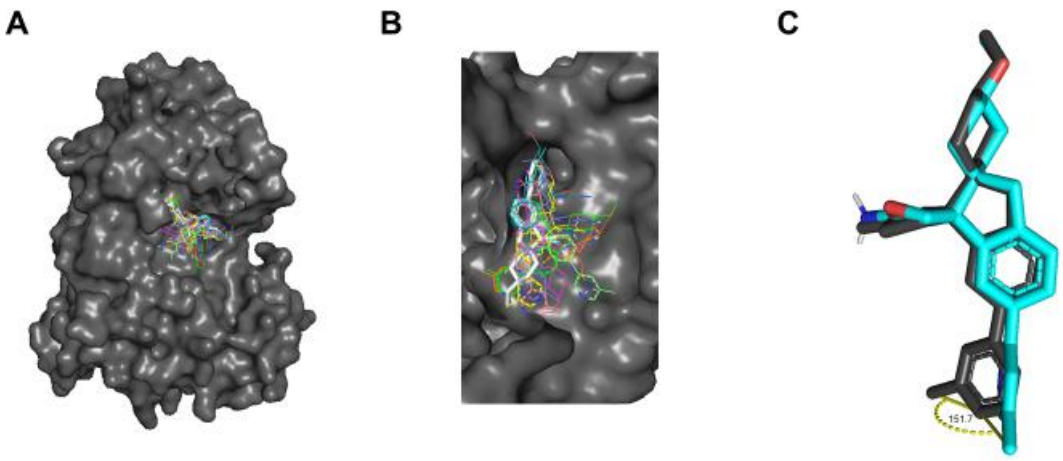

Figure 13: Docking of template native ligand for validation of docking procedure. (A) Representation of eight poses generated by AutoDock Vina when docking B7T inhibitor with prepared template. **(B)** Close view of the eight poses positioned in the canonical active site of BACE1. Orientation of the model with the superior binding affinity is shown in white. **(C)** Alignment of binding orientation of co-crystallised ligand and top scoring docking result.

BACE1 inhibitor C3 was docked in the BACE1 isoform models and the results were analysed in discovery studio visualisation software. Results demonstrate only small variations in affinity between the different isoforms when binding C3, ranging from 8.2 to 9.2 Kcal/mol across the six isoforms. Each model used at least one of the BACE1 key residues, with tyrosine-71 being used most frequently in all but the BACE1-C model. Number of hydrogen bonds and total interactions between models and template appear to have no correlation with the affinity score (Figure 14 and Table 5).

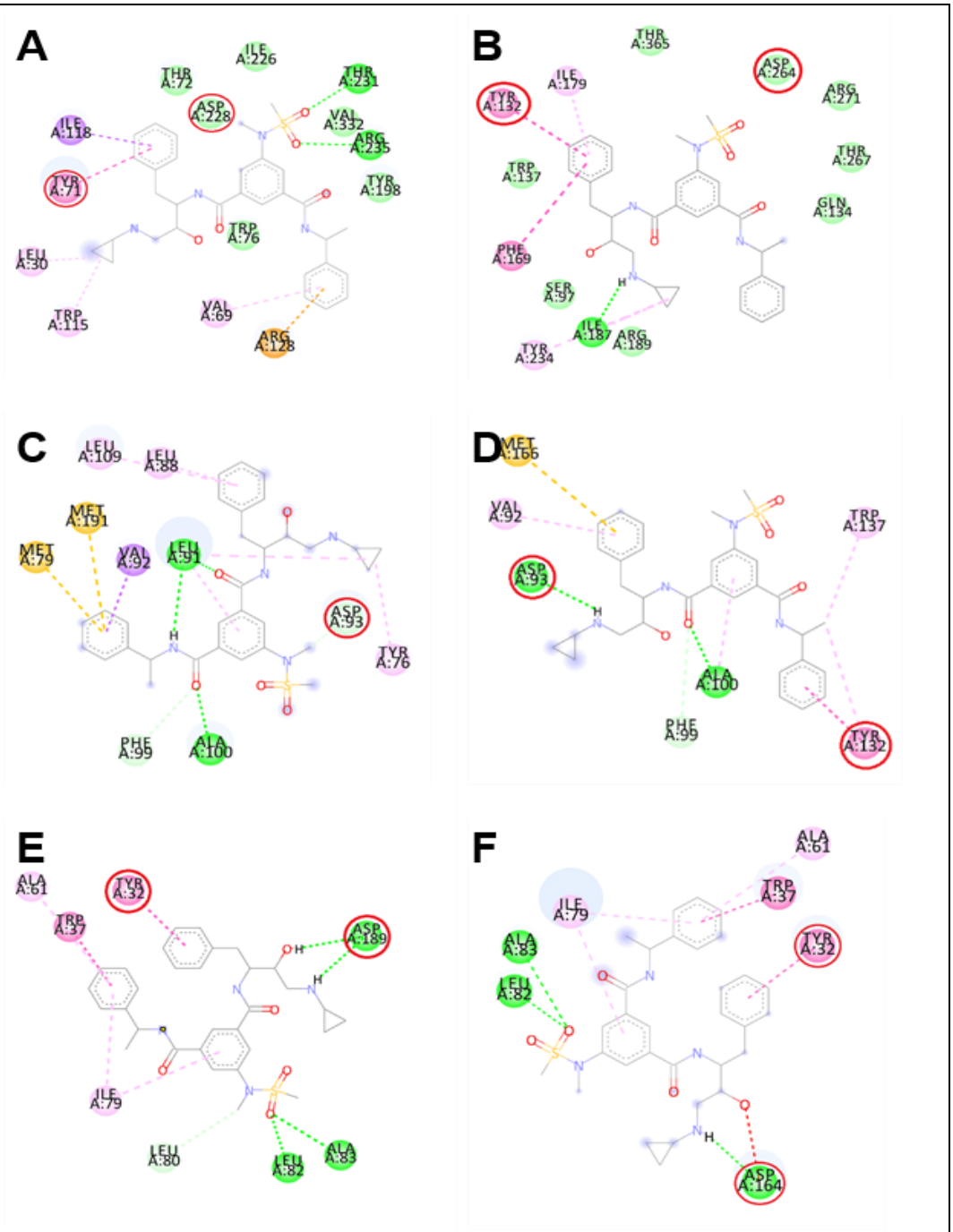

Figure 14: 2D maps of interactions between C3 inhibitor and BACE1 isoform homology-models. (A) Interactions between C3 inhibitor and BACE1-A. **(B)** Interactions between C3 inhibitor and BACE1-B. **(C)** Interactions between C3 inhibitor and BACE1-C. **(D)** Interactions between C3 inhibitor and BACE1-D. **(E)** Interactions between C3 inhibitor and BACE1-5. **(F)** Interactions between C3 inhibitor and BACE1-6. Key binding residues circled in red.

Table 5: BACE1 isoforms docked with C3 inhibitor

Protein	Affinity (Kcal/mol)	Key binding residues utilised			Number of Hydrogen bonds	Total number of contacts
		D32	Y71	D228		
BACE1-A	-8.8		✓	✓	2	14
BACE1-B	-8.7		✓	✓	1	13
BACE1-C	-8.5	✓			3	10
BACE1-D	-8.2	✓	✓		2	7
BACE1-5	-8.9	Missing	✓	✓	4	8
BACE1-6	-9.2	Missing	✓	✓	3	7

8.2.2. Docking of insulin receptor and APP cleavage octapeptide

The known octapeptide cleavage sequence of APP and a predicted octapeptide cleavage sequence of IR was docked with the BACE1 isoform models. The IR octapeptide was generated by Johnson, Chambers and Jayasundera (2013) using an algorithm designed to predict BACE1 substrates, algorithm output was validated against known BACE1 substrates. Docking was done using HPEPDOCK and results were analysed in discovery studio.

Visualisation of the top ten IR octapeptide poses, generated by HPEPDOCK, for all isoform models are distributed within the BACE1 active site. There is less variation in position and orientation of the IR octapeptide poses in BACE1-A, with this uniformity decreasing in BACE1 models B, C and D. Subsequently, uniformity of pose orientation and position is restored in BACE1 isoform 5 and 6 (Figure 15).

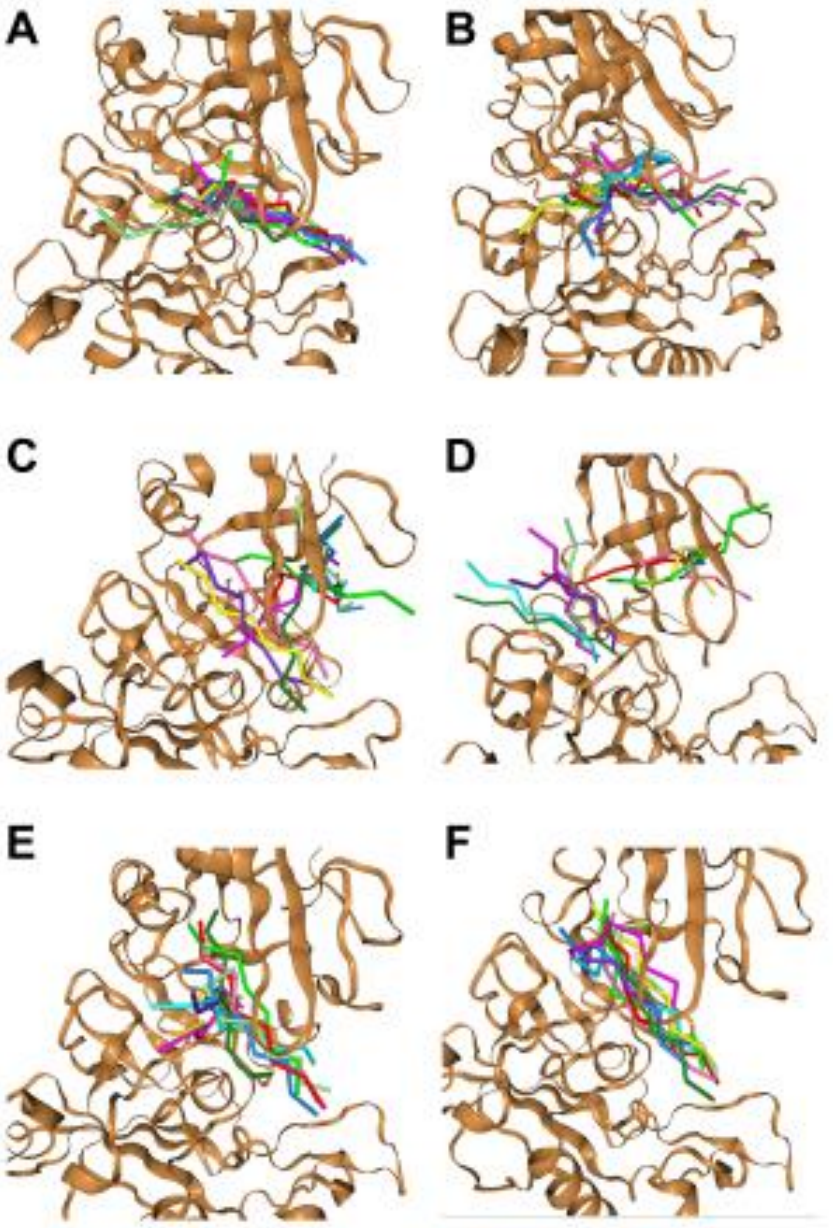

Figure 15: Top ten binding poses of IR motif when docked with BACE1 isoforms. (A) Docking of IR motif in BACE1-A. **(B)** Docking of IR motif in BACE1-B. **(C)** Docking of IR motif in BACE1-C. **(D)** Docking of IR motif in BACE1-D. **(E)** Docking of IR motif in BACE1-5. **(F)** Docking of IR motif in BACE1-6. Receptor and IR motif are shown in brown and rainbow colours respectively in all images.

There is little variation between the docking scores of the BACE1 isoforms when docked with the IR octapeptide; with scores ranging from -224.466 to -263.084

(Table 6). All isoform models interact with at least one of the BACE1 key catalytic residues with tyrosine-71 being used most frequently in all but the BACE1-D model. Number of hydrogen bonds and total interactions between isoform models and the IR octapeptide appear to corelate with the docking score; an increase in hydrogen bonds and total interactions is indicated by an increase in docking score (Table 6 and Figure 16).

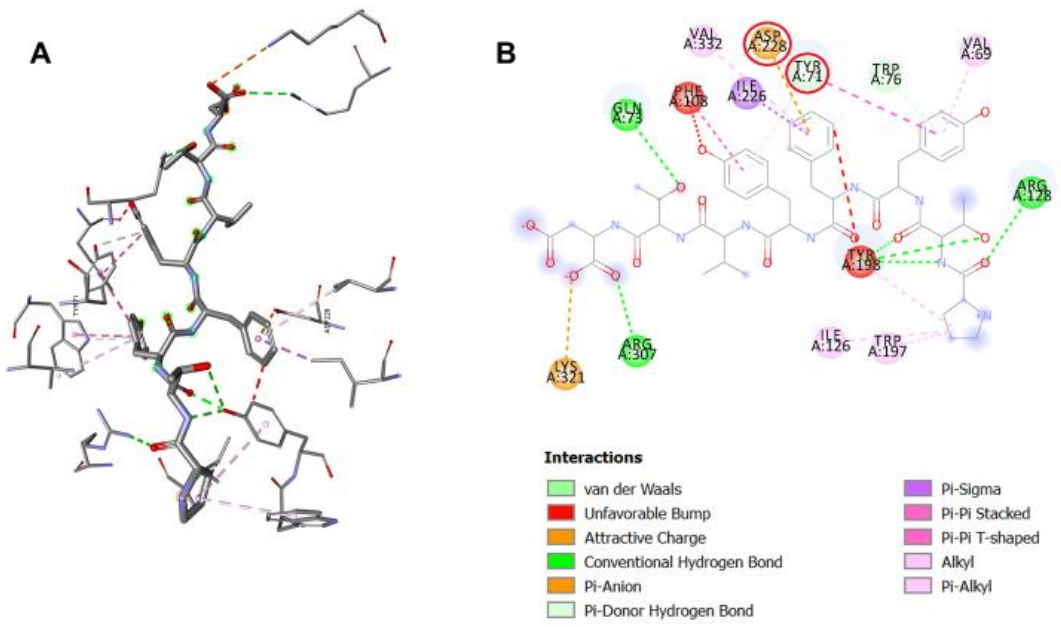

Figure 16: Docking of insulin receptor cleavage motif with BACE1-A. (A) 3D rendering of most energetically favourable binding mode of IR motif. **(B)** 2D receptor (BACE1-A) ligand (IR motif) interaction map. Key binding residues are circled in red. Images created in BIOVIA Discovery Studio.

Table 6: BACE1 isoforms docked with IR peptide motif.

Protein	Docking score	Key binding residues utilised			Number of Hydrogen bonds	Total number of contacts
		D32	Y71	D228		
BACE1-A	-249.720		✓	✓	6	20
BACE1-B	-246.984		✓		3	12
BACE1-C	-224.466	✓	✓		3	10
BACE1-D	-244.063	✓			2	11
BACE1-5	-263.084	Missing	✓		6	20
BACE1-6	-241.002	Missing	✓		2	14

Distribution of the top ten APP poses for each BACE1 isoform model vary considerably in both orientation and position of binding. Both BACE1 isoform models A and D have APP poses that are bound to an allosteric site (Figure 17). The top ten APP binding poses are far more disorganised that those generated from the binding of IR (Figure 16).

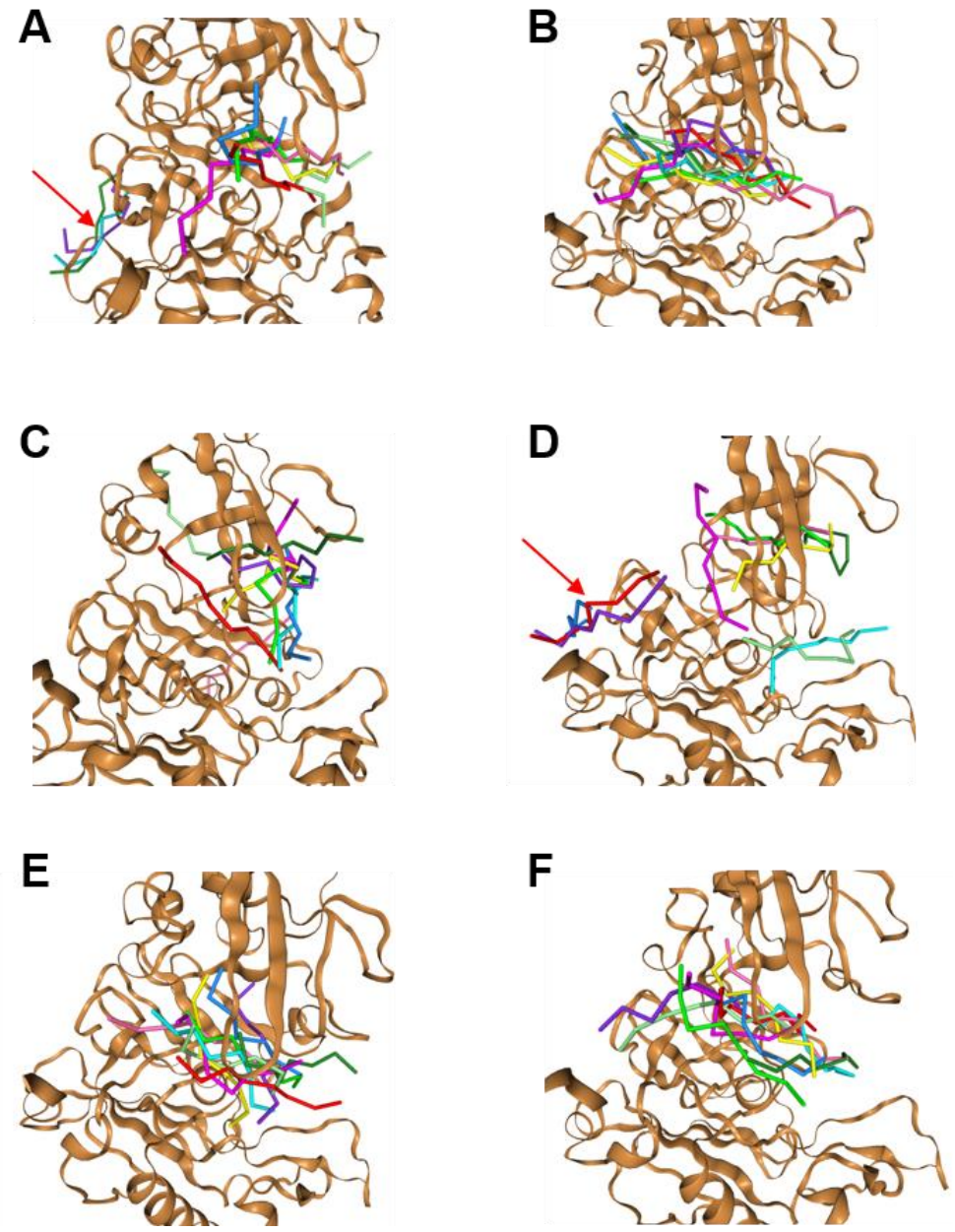

Figure 17: Top ten binding poses of APP motif when docked with BACE1 isoforms. (A) Docking of APP motif in BACE1-A. **(B)** Docking of APP motif in BACE1-B. **(C)** Docking of APP motif in BACE1-C. **(D)** Docking of APP motif in BACE1-D. **(E)** Docking of APP motif in BACE1-5. **(F)** Docking of APP motif in BACE1-6.

Receptor and APP motif are shown in brown and rainbow colours respectively in all images. Red arrows in **(A)** and **(D)** indicate poses bound to an allosteric site.

Docking scores for BACE1 isoform models docked with the APP octapeptide show little variation between isoforms, with scores ranging from 142.905 to 158.473. However, the average of the isoform docking sore, when docked with the APP octapeptide, is 93.48 lower than the average docking score of the IR octapeptide dockings. BACE1 isoforms show high variability in interactions of the key residues with the APP octapeptide with isoforms B and 5 having no interactions and isoform D interacting with all three key residues. Hydrogen bond and total interactions show no correlation with the docking score (Figure 18 and Table 7). When compared with results from the IR docking simulations (Table 6) it is observable that the IR octapeptide forms more interactions with the BACE1 key residues than the APP octapeptide (Table 7).

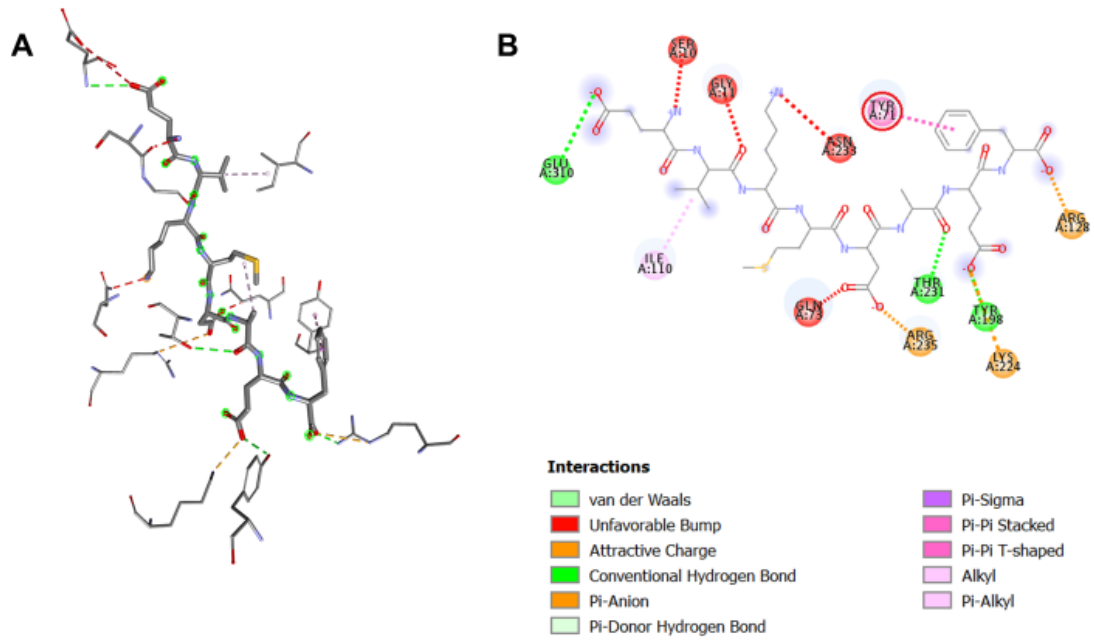

Figure 18: Docking of APP cleavage motif with BACE1-A. (A) 3D rendering of most energetically favourable binding mode of APP motif. **(B)** 2D receptor (BACE1-A) ligand (APP motif) interaction map. Key binding residues are circled in red. Images created in BIOVIA Discovery Studio.

Table 7: BACE1 isoforms docked with APP peptide motif.

Protein	Docking score	Key binding residues utilised			Number of Hydrogen bonds	Total number of contacts
		D32	Y71	D228		
BACE1-A	-158.473		✓		3	12
BACE1-B	-167.048				6	21
BACE1-C	-144.170	✓			4	9
BACE1-D	-151.285	✓	✓	✓	4	17
BACE1-5	-142.905	Missing			3	9
BACE1-6	-144.544	Missing		✓	1	11

9. Discussion

The current lack of treatment for VaD brings into focus the need for new therapeutic targets. Correlation of insulin resistance with vascular diseases, AD and cognitive impairment coupled with the validation of the insulin receptor as a BACE1 substrate leads to the question; does BACE1 regulate insulin signalling and its downstream vascular effects? The current research has established that BACE1 inhibition and knockout increases phosphorylation of Akt and eNOS in ECs both stimulated and not stimulated with insulin; suggesting that BACE1 may exert its effects independently of insulin.

9.1. Inhibition of BACE1 increases Akt and eNOS phosphorylation in peripheral ECs

Zhang et al (2018) demonstrated that inhibition of eNOS with N^{ω}-nitro L-arginine methyl ester (L-NAME) both increased BACE1 and reduced P-eNOS expression in the hippocampus and cortex of stroke-prone spontaneously hypertensive rats in comparison with the control. Furthermore, it has been shown that inhibition of eNOS in human brain microvascular ECs significantly increases expression of BACE1 and APP (Austin, Santhanam and Katusic, 2010). More recently, Meakin et al (2020) have established that endothelial dysfunction, measured by change in perfusion as a function of endothelial dependent acetylcholine action, is reduced in $BACE1^{-/-}$ mice and reversed in obese mice treated with the BACE1 inhibitor C3. Together these studies support the current finding that BACE1 knockout and inhibition increases P-Akt and P-eNOS activity in peripheral ECs at a basal level, independently of insulin stimulation. Specifically, genotype is a significant contributor to the differences in P-Akt and P-eNOS expression in peripheral ECs (Figure 5 and 6). Increased Akt and eNOS expression in $BACE1^{-/-}$ ECs is mirrored in ECs treated with C3 (BACE1 inhibitor), with the presence of C3 making significant contributions to expression

differences of Akt and eNOS (Figure 7 and 8). These findings suggest that the inhibition of BACE1 activity increases insulin mediated eNOS signalling and subsequently has the potential to ameliorate endothelial dysfunction by improvements in vasodilation and reductions in inflammation and oxidative stress. As ECs line the entire vasculature, they permeate all bodily systems and therefore endothelial dysfunction has been closely linked to and cited as a precursor to the clinical onset of several conditions such as, T2DM, atherosclerosis and hypertension (Endemann and Schiffrin, 2004). Therefore, improvements in endothelial function mediated by the inhibition of BACE1, as described here, could help prevent the development and improve the outcome of theses potentially life limiting diseases.

9.2. BACE1 inhibition improves insulin sensitivity

The current work aimed to investigate the link between insulin resistance and BACE1 activity in peripheral ECs. Largely, the current body of literature focuses on the use of skeletal muscle in the investigation of this link. Insulin resistance is characterised by a reduction in IR at the cell surface leading to reduced insulin sensitivity, as defined by a reduction in glucose uptake (Chen et al, 2019). BACE1 has been shown to cleave the IR thus decreasing insulin sensitivity (Meakin et al, 2018); meaning any inhibition of BACE1 activity should result in increased insulin mediated signalling activity, as described here. Results demonstrate a significant contribution of insulin stimulation to the increase in phosphorylation of both Akt and eNOS in a dose dependent manner, with greater phosphorylation levels detected in $BACE1^{-/-}$ and C3 treated ECs. Demonstrating improved insulin sensitivity in $BACE1^{-/-}$ and C3 treated ECs. Current findings are in line with previous work describing recovery of Akt phosphorylation and IR β-subunit protein levels in murine myotubes co-incubated with palmitate, an inducer of insulin resistance, and C3 compared with

myotubes exposed to palmitate only (Botteri et al, 2018). Under physiological conditions IR modulates the balance between vasoactive compounds such as NO and ET-1, which promotes endothelial health. In insulin resistant states this balance shifts to activate endothelial dysfunction (Rask-Madsen and King, 2007). It has become apparent that insulin resistance and endothelial dysfunction are closely associated and exist together in multiple metabolically driven diseases (Kim et al, 2006). Establishing a mechanistic link between insulin resistance and BACE1 activity in ECs is essential in the advancement of understanding around the development of endothelial dysfunction as BACE1 may be implicit in a vicious cycle of aberrant cellular signalling. Insulin resistance elevates levels of ET-1 causing vasoconstriction and subsequent hypoxic conditions, such conditions increase BACE1 expression which in turn can exacerbate insulin resistance, starting the cycle again (Figure 19). Whilst the current work establishes that both insulin stimulation and BACE1 inhibition or knockout increases insulin signalling transduction it does not present a proven link between BACE1 activity and insulin resistance. In collection of the EC lysate samples analysed here the EC growth media was also collected. In order to validate the link between BACE1 activity and insulin sensitivity theses samples should be analysed for the presence of soluble IR fragments as described by Meakin et al (2018). Concentrations of these fragments should be reduced in the media collected from BACE1$^{-/-}$ and C3 treated ECs, as a reduction in BACE1 activity will mean less cleavage of the IR.

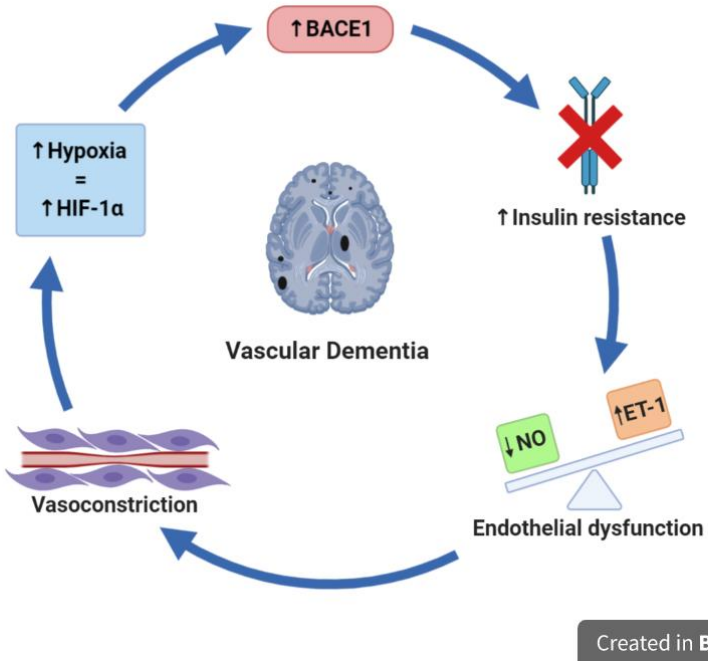

Figure 19: Vicious circle of aberrant cell signalling

Insulin resistance drives an imbalance between NO and ET-1 causing endothelial dysfunction which then leads to vasoconstriction. Vasoconstriction induces hypoxia which elevates expression of HIF-1α**,** a promotor of BACE1, thus increasing BACE1 expression. BACE1 cleaves the insulin receptor exacerbating insulin resistance.

9.3. BACE1 modulation of insulin signalling in BECs is unclear

Data derived from the stimulation of wild type and BACE1$^{-/-}$ BECs with insulin does not reveal any significant changes in insulin signalling between the two genotypes (Figures 9 and 10). Here data collection was halted by the ongoing global pandemic. There are currently large amounts of variation within the data sets and the contribution of genotype to signalling differences is there but not significant. This may be improved by increasing the number of experimental repeats, revealing a clearer picture of the signalling patterns. However, Fu et al (2017) described reductions in hippocampal perfusion, cognition and insulin mediated eNOS signalling in a high fat diet induced rat model of insulin resistance. This suggests

insulin resistance directly effects vascular function in the brain. Additionally, it has been demonstrated in a population cohort study that elevated circulating levels ET-1, increased levels are characteristic of endothelial dysfunction, leads to a higher risk of developing vascular dementia, representing a direct link between endothelial disfunction and VaD (Holm et al, 2017). Furthermore, Meakin et al (2020) established that levels of ET-1 in obese BACE1$^{-/-}$ mice were recovered to levels found in wild type regular chow fed controls. Indicating a role for BACE1 in the homeostasis of endothelial function. Such experimental findings together with the data presented here, regarding increased Akt and eNOS phosphorylation in BACE1$^{-/-}$ and C3 treated peripheral ECs, suggests a plausible role for BACE1 in the pathophysiology of VaD and mixed dementias.

However, results here seem to imply an increase in Akt and eNOS phosphorylation that is independent of insulin stimulation. This may be evidence that BACE1 is affecting Akt and eNOS activation via an alternative pathway. One possible alternative is the vascular endothelial growth factor receptor-1 (VEGF R-1) pathway. Ahmad et al (2006) found that stimulation of VEGF R-1 was responsible for increased phosphorylation of eNOS at Ser1177 and that this increase was mediated via the PI3-K, Akt pathway. Additionally, Cai et al (2012) demonstrated that BACE1 is implicit in the cleavage of VEGF R-1. Together, this could imply that cleavage of VEGF R-1 by BACE1 could reduce endogenous production of NO and that inhibition of BACE1 may ameliorate these effects.

9.4. Evaluation of repurposing BACE1 inhibitors for treatment of VaD

BACE1s apparent action in the endothelium makes it an attractive drug target for the treatment of VaD and mixed dementias as an inhibitor drug would not be

required to cross the BBB in order to exert its effects. There already exists a library of BACE1 inhibitor compounds, abandoned due to their inability to cross the BBB, that could be investigated for their capacity to act at the endothelium (Li et al, 2017). Reducing endothelial dysfunction could conserve cerebral perfusion and protect against cognitive decline. Alternatively, small molecule inhibitors that do cross the BBB that are already in clinical trials may be repurposed. BACE1 has long been a favoured target for the treatment of AD with several small molecule inhibitors in clinical trials. These molecules have been designed to cross the BBB as this is the site of AD pathology (Coimbra et al, 2018). Unfortunately, some trials have been terminated due to a lack of demonstrable improvements in cognition in the subjects and reports of liver toxicity. However, more recent trials in asymptomatic patients have shown promising results in terms of safety, efficacy, and ability to improve cognitive outcomes (Das and Yan, 2019). This implies that it is imperative to treat possible dementia before cognitive impairments become apparent. As safety and efficacy has already been established for some BACE1 inhibitors it would be an efficient and cost-effective process to repurpose such treatments for investigations into their use in VaD.

However, close attention should be paid to dose as BACE1 has been shown to process a number of substrates and chronic inhibition may produce unwanted side-effects. For instance, $BACE1^{-/-}$ mice have demonstrated abnormalities such as hypomyelination and erroneous axon targeting due to the lack of BACE1 cleavage of neuregulin 1 and CHL1 respectively (Vassar, 2016). In contrast, an increase in BACE1 activity leads to Aβ build up that interferes with Ca^{2+} signalling causing a decline in synaptic transmission and plasticity, as observed in AD (Ovsepain et al, 2020). Further to this, the recent review by Ovsepain, Horacek, O'Leary and Hoschl (2020) advocates the hypothesis that BACE1 concentrations in the body must be

maintained in equilibrium and that fluctuations in either direction will have pathological implications.

9.5. Future directions

Here we have described increased eNOS and Akt phosphorylation when BACE1 is inhibited either genetically or pharmacologically in peripheral ECs collected from healthy wildtype or BACE1$^{-/-}$ mice (Figures 5, 6, 7 and 8). However, the current work does not consider pathophysiological alterations present in metabolically driven diseases. Previous work has revealed that increased levels of Aβ and BACE1 are present in brain tissues of a diabetic rat model characterised by high blood glucose. Additionally, the same study found that the stimulation of SK-N-MC cells with glucose increased secretions of Aβ and expression of BACE1 and promoted the binding HIF-1α to the BACE1 gene promotor (Lee et al, 2016). Furthermore, Meakin et al (2020) described increased plasma levels of Aβ in both diet induced obese mice and human T2DM subjects corelating with decreased plasma levels of NO and reduced eNOS phosphorylation in peripheral vascular tissues. Moreover, it has been demonstrated that BACE1 expression is increased in individuals with AD, VaD and mixed dementias (Zuliani et al, 2020). Together these findings suggest that metabolic disturbances such as those indicative of T2DM are linked to increases in Aβ levels and BACE1 expression. Importantly, increased BACE1 expression in VaD and mixed dementias together with the findings of reduced eNOS phosphorylation in the peripheral vasculature suggests a role for BACE1 mediated endothelial dysfunction in development and progression of VaD and mixed dementias. Further investigation should seek to delineate the effects of increased BACE1 activity on insulin mediated eNOS signalling in BECs. As a start this could be investigated in a brain derived endothelial cell line such as bEnd.1 over expressing BACE1 and comparing signalling outputs with BACE1 knockout and wild type cells. Additionally,

BECs may be exposed to pathological conditions that are characteristic of VaD such as hypoxia to ascertain the impact of these conditions on BACE1 and eNOS activity. Moreover, transcriptomic and proteomic databases, such as Endo DB which is an endothelial specific transcriptomic database, could be used to search for commonalities in differentially expressed genes between insulin resistant and BACE1 knockout or overexpressing samples. This may give some indication as to potential BACE1 substrates involved in the upregulation of eNOS activity. Further exploration of the links between insulin resistance, endothelial dysfunction and BACE1 activity and its implications for vascular driven dementias should also be investigated in an in vivo model. A carotid artery occlusion mouse model of vascular dementia in tandem with high fat feeding induced insulin resistance could be employed to assess the effects of BACE1 inhibition on cognition, insulin signalling and markers of endothelial dysfunction.

9.6. Limitations of experimental procedures

Most data presented in the current study was collected using western blotting (Figures 5 to 10). The western blot is an established technique employed to detect and quantify proteins of interest and is utilised Widley across the scientific community. As with any methodology western blotting has its limitations (MacPhee, 2010). It is a time-consuming method that involves many interdependent complex steps by which error can be introduced to the results. For instance, loading controls can often appear over saturated as their expression levels are high, leading to overloading of the lanes, thus impeding normalization values. Another technical issue is incomplete transfer of separated proteins to the nitrocellulose membrane which will give inaccurate densiometric readings (Taylor et al, 2013). Care should be taken to optimise the protocol to the specific experiment and each step should be

followed meticulously to reduce error. Results obtained from western blotting could also be corroborated using an alternative method. In the current study the phosphorylation of eNOS was quantified in wild type and BACE1$^{-/-}$ ECs. These findings may be validated by assessing the activity eNOS by using radiolabelled L-arginine that will be converted to radiolabelled citrulline by activated eNOS. Subsequently, the radiolabelled citrulline product may be separated by ion-exchange and quantified as described by Knowles and Salter (1998).

9.7. Brain ECs can be used in angiogenic sprouting assays

In order to assess the functional implications of BACE1 activity in the cerebral vasculature the fibrin gel bead assay was investigated for its use with primary murine BECs (Figure 11). The current literature does not hold evidence for the use of primary murine BECs in the fibrin gel bead assay. The fibrin gel bead assay usually utilises HUVECs in the study of angiogenesis; the formation of new blood vessels from the existing vasculature, this can be considered a functional metric of endothelial health. Hypoxia is a significant promoter of angiogenesis in vivo (Krock, Skuli and Simon, 2011). Vascular dementia is hallmarked by reduced cerebral blood flow and has been associated with endothelial dysfunction and insulin resistance (Stoeckel et al, 2016). Therefore, quantifying angiogenic activity mediated by BACE1 dependent insulin signalling will give insight into potential functional implications of signalling differences. Here we have described a pilot study whereby primary murine BECs were used to coat Cytodex beads under control conditions (Figure 11). Results demonstrate that BECs coat the beads and go on to form sprouts. Sprout number in the current work ranges from ≈ 4 to 6 sprouts per bead this is comparable to a study by Jury et al (2020) who reported an average spout number per bead of ≈ 4 in control conditions. This study also recorded an average sprout length of ≈ 200µm in control conditions this is more than double the range of

lengths recorded here of ≈ 55 to 75µm. However, another study investigating the effects of VEGF concentrations on the bead sprouting assay found the average sprout length at 0.5 ng/ml VEGF (the concentration used here) to be ≈ 90µm; this result is similar to that reported here (Nakatsu et al, 2003). However, the specialisation of ECs in order to form the BBB may be lost in the cell culture process as this specialisation is induced by neighbouring cell types such as astrocytes (Janzer and Raff, 1987). Azam et al (2018) describes a method for sequentially coating Cytodex bead with ECs then pericytes, this method could be adapted for the incorporation of astrocytes in order to maintain brain specific EC specialisation.

9.8. BACE1 isoforms show no significant preference for C3 inhibitor

BACE1 has six known isoforms to date. These isoforms have been demonstrated to be differentially expressed in a tissue, age and disease dependent manor. For instance, BACE1-C has been shown to be absent in expression in the cerebellum but highly expressed in the frontal cortex and its expression levels change with age (Zohar et al, 2003) (Holsinger et al, 2013). However, this topic is scarcely represented in the literature and there is currently no evidence as to the expression patterns of BACE1 isoforms in endothelial tissues. Currently only the Crystal structure for BACE1-A, the canonical sequence, has been solved. Given these differences in expression an investigation into the interactions between the inhibitor employed in the current work, C3, and the BACE1 isoforms was carried out using homology models of the BACE1 isoforms. Results obtained from docking of C3 with the isoform homology models revealed little difference in affinity between C3 and the different isoforms with affinities ranging from 8 .2 to 9.2 Kcal/mol across all isoforms. The most well characterised isoforms are BACE1-A, B, C and D; taking this into account the affinities range from 8.2 to 8.8 Kcal/mol, an even smaller range (Figure 14). These minimal differences in affinity may be substrate dependent as

one study demonstrated that BACE1-B demonstrated no APP processing where another demonstrated APP processing at 73% of that BACE1-A using APP and the Swedish mutant APP respectively (Holsinger et al, 2013). The similarity in binding affinities presented in the current work still leaves the question of the purpose of the BACE1 isoforms unanswered. As well as the affinity of C3 for the BACE1 isoforms the utilisation of key binding residues by the isoforms was assessed (Figure 14). Across the four main isoforms (BACE1-A to D) all use one of the two aspartic acid residues and three of the isoforms, except BACE1-C, use the tyrosine-71 residue. The utilisation of these key residues indicates that the inhibitor is well located within the binding site. However, BACE1 catalytic capacity is derived from the simultaneous use of the two aspartic acid residues, whereas the models reported here only use one or the other. Shimizu et al (2008) describe a conserved water molecule that sits between the aspartic acid residues, that contributes to the catalytic activity of BACE1 by allowing APP cleavage by hydrolysis. The models reported here had their water molecules removed in preparation for docking; it may be interesting to investigate inhibitor binding in relation to the utilisation of the aspartic acid residues in homology models with the conserved water molecule in place. Despite homology modelling being the most accurate way to predict a protein structure they are seldom completely accurate when compared with experimentally derived structures. However, homology modelling is becoming increasingly accurate and is widely used in drug design and protein engineering applications, among others and is considered the most accurate procedure for modelling of unknown protein structures (Gupta, Akhtar and Bajpai, 2014). To further asses the validity of the results presented here the docking simulation and modelling could be carried out across multiple servers and results compared for similarities and differences.

9.9. APP and the insulin receptor as BACE1 substrates: an overview

Insulin resistance has been closely associated with VaD, and T2DM is a risk factor for the development of VaD (Doney et al, 2019). As demonstrated in the current work, along with work by Meakin et al (2018) revealing cleavage of the insulin receptor by BACE1, insulin signalling may be modulated by BACE1 activity. APP is thought of as the main substrate of BACE1 due to its role in the pathogenies of AD. Here we investigate how BACE1 interacts with both the insulin receptor and APP in order to offer insight into the favourability of BACE1 to these substrates. The known octapeptide sequence of APP and a predicted octapeptide sequence of the insulin receptor BACE1 cleavage sites were blind docked using a peptide specific docking server. Octapeptides were docked with models of all BACE1 isoforms. However, here we discuss only the results of BACE1-A as this is the most abundant and well characterised isoform.

9.10. Insulin receptor is a better predicted substrate for BACE1

The docking score, a measure of protein-ligand affinity, for BACE1-A with the insulin receptor octapeptide was -249.720, interestingly the docking score for the APP octapeptide was 63% higher at -148.473, where a more negative docking score represents greater enzyme-substrate affinity (Table 6 and 7). The superior docking score of the insulin receptor octapeptide is likely due to receptor-substrate bonds formed. The most energetically favourable insulin receptor octapeptide pose forms six hydrogen bonds and twenty bonds overall wit BACE1, whilst the APP octapeptide forms only three hydrogen bonds with twelve bonds overall. In addition, the distribution of the top ten poses of the APP octapeptide are more loosely distributed within the active site of BACE1 in comparison with the top ten poses of the insulin receptor octapeptide, which are tightly centred within the active site

(Figure 15 and 17). Also, three of the binding poses of the APP octapeptide are bound to an allosteric site. Another point of note is the APP octapeptide only utilises the tyrosine-71 key residue and neither of the two catalytic aspartic acid residues; on the other hand, the insulin receptor octapeptide forms bonds with tyrosine-71 and aspartic acid-228. These observations demonstrate the preference of BACE1 for the insulin receptor peptide motif. As APP is the most well-known and intensively investigated BACE1 substate it could have been expected that it would show a more favourable affinity to BACE1. The potential higher affinity of the insulin receptor to BACE1 underpins the currently poor characterisation of BACE1 functions outside of Aβ production in AD. Using an algorithm, validated against known BACE1 substrates, Johnson, Chambers and Jayasundera (2013) revealed 962 putative BACE1 substrates with predicted cleavage recognition sites, including the insulin receptor octapeptide motif used here. So many potential BACE1 substrates corroborates BACE1 loose substrate specificity. Future work may seek to offer insight into the physiological roles of BACE1 by characterising the interactions between putative substrates and BACE1 in molecular docking simulations.

9.11. Limitations of computational modelling

Work done here is limited by the use of a predicted cleavage motif of the insulin receptor; this octapeptide motif has not been fully validated experimentally. However, Meakin et al (2018) demonstrated that a similar peptide was invitro cleaved at the predicted site by detecting the peptide fragments via RP-HPLC. Another limitation of the docking results presented in the current work is the use of octapeptide motifs as a representation of the full protein structure. This approach was taken due to the lack of full 3D protein structures of both the insulin receptor and APP in the PDB, crucially in both instances the juxta membrane domains containing the BACE1 cleavage sequence is missing in all PDB structures. Due to

the environment of juxta membrane domains, they are notoriously difficult to capture by x-ray crystallography and the subsequent lack of solved structures for these domain localities makes them difficult to model (De Brevern, 2011). Whilst results demonstrate a superior affinity between BACE1 and the insulin receptor it does not account for the structural and conformational factors that will inevitably affect the protein-protein interaction. For instance, the insulin receptor consists of 1382 amino acids whilst APP is made up of only 770 amino acids (Stelzer et al, 2016), this difference in size will contribute to the protein-protein binding dynamics. Another factor to consider is the dramatic conformational changes of the insulin receptor upon the binding of insulin, as described by Scapin et al (2018). It maybe that such large-scale conformational changes may lead to the favouring of either the substrate bound or unbound insulin receptor structure by BACE1. Future work should look toward resolving the full-length structure of the insulin receptor and APP using transmembrane structure prediction tools to model the uncharacterised juxta membrane locations. The full-length insulin receptor and APP models may then be used in protein-protein docking simulations in order to more accurately characterise the interactions between BACE1 and APP and the insulin receptor.

10. Conclusions

The current lack of treatment options for VaD makes it imperative to identify new potential targets for the development of therapeutics to improve disease management and progression. BACE1 activity has been shown to be concomitant in insulin resistance and endothelial dysfunction, both of which are characteristic pathologies in VaD. The current work seeks to add insight into the potential link between BACE1 activity and insulin mediated Akt and eNOS signalling, which is important for vascular health. Results reported here demonstrate that genetic and pharmacological inhibition of BACE1 has a significant enhancing impact on the

phosphorylation of Akt and eNOS in peripheral ECs. However, evidence for BACE1 mediated increases in P-Akt and P-eNOS expression in BECs remains unclear as data collection is incomplete. Such demonstrable improvements suggest BACE1 may be a suitable target for the treatment and management of peripheral diseases with underlying endothelial dysfunction. Should results in BECs follow the same pattern of improved Akt and eNOS phosphorylation then BACE1 may considered as a plausible drug target for the treatment of cerebrovascular impairments. Further investigation is required to validate the role of BACE1 in the signalling differences observed here via the detection of cleaved insulin receptor fragments in the EC growth media. Additionally, the effects of BACE1 overexpression on signalling should be investigated given that many pathologies display increased BACE1 activity. Overall, the current work has offered valuable insight into the relationship between BACE1 activity and insulin mediated Akt and eNOS signalling in the endothelium. With potential importance for the development of new therapeutics for the management of peripheral and cerebral vascular impairments via the repurposing of BACE1 inhibitor molecules already in clinical trials.

11. References

Abbott, N.J., Patabendige, A.A., Dolman, D.E., Yusof, S.R. and Begley, D.J., 2010. Structure and function of the blood–brain barrier. *Neurobiology of disease*, *37*(1), pp.13-25.

Altschul, S.F., Gish, W., Miller, W., Myers, E.W. and Lipman, D.J., 1990. Basic local alignment search tool. *Journal of molecular biology*, *215*(3), pp.403-410.

American Diabetes Association, 2007. Soluble insulin receptor ectodomain is elevated in the plasma of patients with diabetes mellitus. *Diabetes*.

Araki, W., 2016. Post-translational regulation of the β-secretase BACE1*. Brain research bulletin,* 126, pp.170-177.

Arnold, S.E., Arvanitakis, Z., Macauley-Rambach, S.L., Koenig, A.M., Wang, H.Y., Ahima, R.S., Craft, S., Gandy, S., Buettner, C., Stoeckel, L.E. and Holtzman, D.M., 2018. Brain insulin resistance in type 2 diabetes and Alzheimer disease: concepts and conundrums. *Nature Reviews Neurology*, *14*(3), pp.168-181.

Austin, S.A., Santhanam, A.V. and Katusic, Z.S., 2010. Endothelial nitric oxide modulates expression and processing of amyloid precursor protein. *Circulation research*, *107*(12), pp.1498-1502.

Barão, S., Moechars, D., Lichtenthaler, S.F. and De Strooper, B., 2016. BACE1 physiological functions may limit its use as therapeutic target for Alzheimer's disease. *Trends in neurosciences*, 39(3), pp.158-169.

Beckman, J.A. and Creager, M.A., 2016. Vascular complications of diabetes. *Circulation research*, 118(11), pp.1771-1785.

Bernard-Patrzynski, F., Lécuyer, M.A., Puscas, I., Boukhatem, I., Charabati, M., Bourbonnière, L., Ramassamy, C., Leclair, G., Prat, A. and Roullin, V.G., 2019. Isolation of endothelial cells, pericytes and astrocytes from mouse brain. *PloS one*, *14*(12), p.e0226302.

BIOVIA, Dassault Systèmes., 2020. BIOVIA Discovery Studio, Version 20.1, San Diego: Dassault Systèmes

Botteri, G., Salvadó, L., Gumà, A., Hamilton, D.L., Meakin, P.J., Montagut, G., Ashford, M.L., Ceperuelo-Mallafré, V., Fernández-Veledo, S., Vendrell, J. and Calderón-Dominguez, M., 2018. The BACE1 product sAPPβ induces ER stress and inflammation and impairs insulin signaling. *Metabolism*, *85*, pp.59-75.

Brüning, J.C., Gautam, D., Burks, D.J., Gillette, J., Schubert, M., Orban, P.C., Klein, R., Krone, W., Müller-Wieland, D. and Kahn, C.R., 2000. Role of brain insulin

receptor in control of body weight and reproduction. *Science*, *289*(5487), pp.2122-2125.

Bu, G., Liu, C.C. and Kanekiyo, T., 2013. Vascular hypothesis of Alzheimer's disease: role of apoE and apoE receptors. *Molecular Neurodegeneration*, *8*(S1), p.O20.

Busche, M.A. and Hyman, B.T., 2020. Synergy between amyloid-β and tau in Alzheimer's disease. *Nature Neuroscience*, *23*(10), pp.1183-1193.

Coimbra, J.R., Marques, D.F., Baptista, S.J., Pereira, C.M., Moreira, P.I., Dinis, T.C., Santos, A.E. and Salvador, J.A., 2018. Highlights in BACE1 inhibitors for Alzheimer's disease treatment. *Frontiers in chemistry*, *6*, p.178.

CDC. 2020. *Types of Stroke.* [Online]. [Accessed 28 October 2020]. Available from: https://www.cdc.gov/stroke/types_of_stroke.htm

Chen, Y., Huang, L., Qi, X. and Chen, C., 2019. Insulin receptor trafficking: consequences for insulin sensitivity and diabetes*. International journal of molecular sciences*, 20(20), p.5007.

Choi, K. and Kim, Y.B., 2010. Molecular mechanism of insulin resistance in obesity and type 2 diabetes. *The Korean journal of internal medicine*, 25(2), p.119.

Christensen, M.A., Zhou, W., Qing, H., Lehman, A., Philipsen, S. and Song, W., 2004. Transcriptional regulation of BACE1, the β-amyloid precursor protein β-secretase, by Sp1. *Molecular and cellular biology*, 24(2), pp.865-874.

Chui, H.C., 2007. Subcortical ischemic vascular dementia. *Neurologic clinics*, 25(3), pp.717-740.

Cimino, M., Gelosa, P., Gianella, A., Nobili, E., Tremoli, E. and Sironi, L., 2007. Statins: multiple mechanisms of action in the ischemic brain. *The Neuroscientist*, *13*(3), pp.208-213.

Croll, T.I., Smith, B.J., Margetts, M.B., Whittaker, J., Weiss, M.A., Ward, C.W. and Lawrence, M.C., 2016. Higher-resolution structure of the human insulin receptor ectodomain: multi-modal inclusion of the insert domain*. Structure*, 24(3), pp.469-476.

Czech, M.P., 2017. Insulin action and resistance in obesity and type 2 diabetes. *Nature medicine*, 23(7), pp.804-814.

Das, B. and Yan, R., 2019. A close look at BACE1 inhibitors for Alzheimer's disease treatment. *CNS drugs*, *33*(3), pp.251-263.

De Brevern, A.G., 2010. 3D structural models of transmembrane proteins. In *Membrane Protein Structure Determination* (pp. 387-401). Humana Press, Totowa, NJ.

DeLano, W.L., 2002. Pymol: An open-source molecular graphics tool. *CCP4 Newsletter on protein crystallography*, *40*(1), pp.82-92.

Dodd, G.T. and Tiganis, T., 2017. Insulin action in the brain: Roles in energy and glucose homeostasis. *Journal of neuroendocrinology*, *29*(10), p.e12513.

Doney, A.S., Bonney, W., Jefferson, E., Walesby, K.E., Bittern, R., Trucco, E., Connelly, P., McCrimmon, R.J. and Palmer, C.N., 2019. Investigating the Relationship Between Type 2 Diabetes and Dementia Using Electronic Medical Records in the GoDARTS Bioresource. *Diabetes Care*, *42*(10), pp.1973-1980.

Endemann, D.H. and Schiffrin, E.L., 2004. Endothelial dysfunction. *Journal of the American Society of Nephrology*, *15*(8), pp.1983-1992.

Exalto, L.G., Whitmer, R.A., Kappele, L.J. and Biessels, G.J., 2012. An update on type 2 diabetes, vascular dementia and Alzheimer's disease. *Experimental gerontology*, 47(11), pp.858-864.

Fadini, G.P., Albiero, M., Bonora, B.M. and Avogaro, A., 2019. Angiogenic abnormalities in diabetes mellitus: mechanistic and clinical aspects. *The Journal of Clinical Endocrinology & Metabolism,* 104(11), pp.5431-5444.

Fishilevich, S., Nudel, R., Rappaport, N., Hadar, R., Plaschkes, I., Iny Stein, T., Rosen, N., Kohn, A., Twik, M., Safran, M. and Lancet, D., 2017. GeneHancer: genome-wide integration of enhancers and target genes in GeneCards. Database, 2017.

Fu, Z., Wu, J., Nesil, T., Li, M.D., Aylor, K.W. and Liu, Z., 2017. Long-term high-fat diet induces hippocampal microvascular insulin resistance and cognitive dysfunction. *American Journal of Physiology-Endocrinology and Metabolism*, *312*(2), pp.E89-E97.

Garlanda, C. and Dejana, E., 1997. Heterogeneity of endothelial cells: specific markers. *Arteriosclerosis, thrombosis, and vascular biology*, *17*(7), pp.1193-1202.

Girouard, H. and Munter, L.M., 2018. The many faces of vascular cognitive impairment. *Journal of neurochemistry*, *144*(5), pp.509-512.

Godsland, I.F., 2010. Insulin resistance and hyperinsulinaemia in the development and progression of cancer. *Clinical science*, 118(5), pp.315-332.

Gupta, C.L., Akhtar, S. and Bajpai, P., 2014. In silico protein modeling: possibilities and limitations. *EXCLI journal*, *13*, p.513.

Holm, H., Nägga, K., Nilsson, E.D., Ricci, F., Melander, O., Hansson, O., Bachus, E., Magnusson, M. and Fedorowski, A., 2017. Biomarkers of microvascular endothelial dysfunction predict incident dementia: a population-based prospective study. *Journal of Internal Medicine*, *282*(1), pp.94-101.

Holsinger, R.D., Goense, N., Bohorquez, J. and Strappe, P., 2013. Splice variants of the Alzheimer's disease beta-secretase, BACE1. *Neurogenetics*, 14(1), pp.1-9.

Hu, X., Hicks, C.W., He, W., Wong, P., Macklin, W.B., Trapp, B.D. and Yan, R., 2006. Bace1 modulates myelination in the central and peripheral nervous system. *Nature neuroscience*, 9(12), pp.1520-1525.

Janzer, R.C. and Raff, M.C., 1987. Astrocytes induce blood–brain barrier properties in endothelial cells. *Nature*, *325*(6101), pp.253-257.

Johnson, J.L., Chambers, E. and Jayasundera, K., 2013. Application of a bioinformatics-based approach to identify novel putative in vivo BACE1 substrates. *Biomedical engineering and computational biology*, 5, pp.BECB-S8383.

Jury, D., Daugaard, I., Sanders, K.J., Hansen, L.L., Agalliu, D. and Pedersen, I.M., 2020. miR-151a enhances Slug dependent angiogenesis. *Oncotarget*, *11*(23), p.2160.

Kalaria, R.N., Akinyemi, R. and Ihara, M., 2012. Does vascular pathology contribute to Alzheimer changes?. *Journal of the neurological sciences*, *322*(1-2), pp.141-147.

Kandalepas, P.C. and Vassar, R., 2012. Identification and biology of β-secretase. *Journal of neurochemistry*, 120, pp.55-61.

Karran, E., Mercken, M. and De Strooper, B., 2011. The amyloid cascade hypothesis for Alzheimer's disease: an appraisal for the development of therapeutics. *Nature reviews Drug discovery*, *10*(9), pp.698-712.

Kim, J.A., Montagnani, M., Koh, K.K. and Quon, M.J., 2006. Reciprocal relationships between insulin resistance and endothelial dysfunction: molecular and pathophysiological mechanisms. *Circulation*, *113*(15), pp.1888-1904.

Knowles, R.G. and Salter, M., 1998. Measurement of NOS activity by conversion of radiolabeled arginine to citrulline using ion-exchange separation. In *Nitric oxide protocols* (pp. 67-73). Humana Press.

Koelsch, G., 2017. BACE1 function and inhibition: implications of intervention in the amyloid pathway of Alzheimer's disease pathology*. Molecules*, 22(10), p.1723.

Krock, B.L., Skuli, N. and Simon, M.C., 2011. Hypoxia-induced angiogenesis: good and evil. *Genes & cancer*, *2*(12), pp.1117-1133.

Iadecola, C., 2013. The pathobiology of vascular dementia. *Neuron*, *80*(4), pp.844-866.

Lee, H.J., Ryu, J.M., Jung, Y.H., Lee, S.J., Kim, J.Y., Lee, S.H., Hwang, I.K., Seong, J.K. and Han, H.J., 2016. High glucose upregulates BACE1-mediated Aβ production through ROS-dependent HIF-1α and LXRα/ABCA1-regulated lipid raft reorganization in SK-N-MC cells. *Scientific reports*, *6*(1), pp.1-15.

Li, J.M., Huang, L.L., Liu, F., Tang, B.S. and Yan, X.X., 2017. Can brain impermeable BACE1 inhibitors serve as anti-CAA medicine?. *BMC neurology*, *17*(1), p.163.

Livingston, G., Sommerlad, A., Orgeta, V., Costafreda, S.G., Huntley, J., Ames, D., Ballard, C., Banerjee, S., Burns, A., Cohen-Mansfield, J. and Cooper, C., 2017. Dementia prevention, intervention, and care. *The Lancet*, *390*(10113), pp.2673-2734.

MacPhee, D.J., 2010. Methodological considerations for improving Western blot analysis. *Journal of pharmacological and toxicological methods*, *61*(2), pp.171-177.

Manrique, C., Lastra, G. and Sowers, J.R., 2014. New insights into insulin action and resistance in the vasculature. *Annals of the New York Academy of Sciences*, 1311(1), p.138.

McConnell, H.L., Kersch, C.N., Woltjer, R.L. and Neuwelt, E.A., 2017. The translational significance of the neurovascular unit. *Journal of biological chemistry*, *292*(3), pp.762-770.

McKay, E. and Counts, S.E., 2017. Multi-infarct dementia: a historical perspective. *Dementia and Geriatric Cognitive Disorders Extra*, 7(1), pp.160-171.

Meakin, P.J., Coull, B.M., Tuharska, Z., McCaffery, C., Akoumianakis, I., Antoniades, C., Brown, J., Griffin, K.J., Platt, F., Ozber, C.H. and Yuldasheva, N.Y., 2020. Elevated circulating amyloid concentrations in obesity and diabetes promote vascular dysfunction. *The Journal of Clinical Investigation*.

Meakin, P.J., Mezzapesa, A., Benabou, E., Haas, M.E., Bonardo, B., Grino, M., Brunel, J.M., Desbois-Mouthon, C., Biddinger, S.B., Govers, R. and Ashford, M.L., 2018. The beta secretase BACE1 regulates the expression of insulin receptor in the liver. *Nature communications*, 9(1), pp.1-14.

Mok, V.C., Lam, B.Y., Wong, A., Ko, H., Markus, H.S. and Wong, L.K., 2017. Early-onset and delayed-onset poststroke dementia—revisiting the mechanisms*. Nature Reviews Neurology*, 13(3), pp.148-159.

Muniyappa, R. and Sowers, J.R., 2013. Role of insulin resistance in endothelial dysfunction. *Reviews in Endocrine and Metabolic Disorders*, *14*(1), pp.5-12.

Nakatsu, M.N., Davis, J. and Hughes, C.C., 2007. Optimized fibrin gel bead assay for the study of angiogenesis. *JoVE (Journal of Visualized Experiments)*, (3), p.e186.

Nakatsu, M.N., Sainson, R.C., Pérez-del-Pulgar, S., Aoto, J.N., Aitkenhead, M., Taylor, K.L., Carpenter, P.M. and Hughes, C.C., 2003. VEGF 121 and VEGF 165 regulate blood vessel diameter through vascular endothelial growth factor receptor 2 in an in vitro angiogenesis model. *Laboratory investigation*, *83*(12), pp.1873-1885.

Ovsepian, S.V., Horacek, J., O'Leary, V.B. and Hoschl, C., 2020. The Ups and Downs of BACE1: Walking a Fine Line between Neurocognitive and Other Psychiatric Symptoms of Alzheimer's Disease. *The Neuroscientist*, p.1073858420940943.

Rains, J.L. and Jain, S.K., 2011. Oxidative stress, insulin signaling, and diabetes. *Free Radical Biology and Medicine*, 50(5), pp.567-575.

Román, G.C., 1999. A historical review of the concept of vascular dementia: lessons from the past for the future. Alzheimer disease and associated disorders, 13(3), p.S4.

Román, G.C., Tatemichi, T.K., Erkinjuntti, T., Cummings, J.L., Masdeu, J.C., Garcia, J.H., Amaducci, L., Orgogozo, J.M., Brun, A., Hofman, A. and Moody, D.M., 1993. Vascular dementia: diagnostic criteria for research studies: report of the NINDS-AIREN International Workshop. *Neurology*, *43*(2), pp.250-250.

Scapin, G., Dandey, V.P., Zhang, Z., Prosise, W., Hruza, A., Kelly, T., Mayhood, T., Strickland, C., Potter, C.S. and Carragher, B., 2018. Structure of the insulin receptor–insulin complex by single-particle cryo-EM analysis. *Nature*, 556(7699), pp.122-125.

Shimizu, H., Tosaki, A., Kaneko, K., Hisano, T., Sakurai, T. and Nukina, N., 2008. Crystal structure of an active form of BACE1, an enzyme responsible for amyloid β protein production*. Molecular and cellular biology*, 28(11), pp.3663-3671.

Schneider, C.A., Rasband, W.S. and Eliceiri, K.W., 2012. NIH Image to ImageJ: 25 years of image analysis. *Nature methods*, *9*(7), pp.671-675.

Skrobot, O.A., O'Brien, J., Black, S., Chen, C., DeCarli, C., Erkinjuntti, T., Ford, G.A., Kalaria, R.N., Pantoni, L., Pasquier, F. and Roman, G.C., 2017. The vascular impairment of cognition classification consensus study*. Alzheimer's & Dementia*, 13(6), pp.624-633.

Spronk, S.A. and Carlson, H.A., 2011. The role of tyrosine 71 in modulating the flap conformations of BACE1*. Proteins: Structure, Function, and Bioinformatics*, 79(7), pp.2247-2259.

Stancu, C. and Sima, A., 2001. Statins: mechanism of action and effects. *Journal of cellular and molecular medicine*, *5*(4), pp.378-387.

Stelzer, G., Rosen, N., Plaschkes, I., Zimmerman, S., Twik, M., Fishilevich, S., Stein, T.I., Nudel, R., Lieder, I., Mazor, Y. and Kaplan, S., 2016. The GeneCards suite: from gene data mining to disease genome sequence analyses. *Current protocols in bioinformatics*, *54*(1), pp.1-30.

Stoeckel, L.E., Arvanitakis, Z., Gandy, S., Small, D., Kahn, C.R., Pascual-Leone, A., Pawlyk, A., Sherwin, R. and Smith, P., 2016. Complex mechanisms linking neurocognitive dysfunction to insulin resistance and other metabolic dysfunction. *F1000Research*, *5*.

Su, J.B., 2015. Vascular endothelial dysfunction and pharmacological treatment. *World journal of cardiology*, *7*(11), p.719.

Sun, X., He, G., Qing, H., Zhou, W., Dobie, F., Cai, F., Staufenbiel, M., Huang, L.E. and Song, W., 2006. Hypoxia facilitates Alzheimer's disease pathogenesis by up-regulating BACE1 gene expression*. Proceedings of the National Academy of Sciences,* 103(49), pp.18727-18732.

Taylor, S.C., Berkelman, T., Yadav, G. and Hammond, M., 2013. A defined methodology for reliable quantification of Western blot data. *Molecular biotechnology*, *55*(3), pp.217-226.

Thal, D.R., Grinberg, L.T. and Attems, J., 2012. Vascular dementia: different forms of vessel disorders contribute to the development of dementia in the elderly brain. *Experimental gerontology*, 47(11), pp.816-824.

T O'Brien, J. and Thomas, A., 2015. Vascular dementia. *The Lancet*, *386*(10004), pp.1698-1706.

Trott, O. and Olson, A.J., 2010. AutoDock Vina: improving the speed and accuracy of docking with a new scoring function, efficient optimization, and multithreading. *Journal of computational chemistry*, *31*(2), pp.455-461.

UniProt Consortium, 2019. UniProt: a worldwide hub of protein knowledge. *Nucleic acids research*, *47*(D1), pp.D506-D515.

Van Der Flier, W.M., Skoog, I., Schneider, J.A., Pantoni, L., Mok, V., Chen, C.L. and Scheltens, P., 2018. Vascular cognitive impairment. *Nature Reviews Disease Primers*, *4*(1), pp.1-16.

Vassar, R. and Cole, S.L., 2007. The basic biology of BACE1: A key therapeutic target for Alzheimer's disease. *Current Genomics*, 8(8), pp.509-530.

Wardlaw, J., 2005. What causes lacunar stroke? *Journal of Neurology, Neurosurgery & Psychiatry*

Waterhouse, A., Bertoni, M., Bienert, S., Studer, G., Tauriello, G., Gumienny, R., Heer, F.T., de Beer, T.A.P., Rempfer, C., Bordoli, L. and Lepore, R., 2018. SWISS-MODEL: homology modelling of protein structures and complexes. *Nucleic acids research*, *46*(W1), pp.W296-W303.

Wimo, A., Guerchet, M., Ali, G.C., Wu, Y.T., Prina, A.M., Winblad, B., Jönsson, L., Liu, Z. and Prince, M., 2017. The worldwide costs of dementia 2015 and comparisons with 2010. *Alzheimer's & Dementia*, *13*(1), pp.1-7.

Wolters, F.J. and Ikram, M.A., 2019. Epidemiology of vascular dementia: nosology in a time of epiomics. *Arteriosclerosis, thrombosis, and vascular biology*, 39(8), pp.1542-1549.

Yaribeygi, H., Farrokhi, F.R., Butler, A.E. and Sahebkar, A., 2019. Insulin resistance: Review of the underlying molecular mechanisms. *Journal of cellular physiology*, 234(6), pp.8152-8161.

Zekry, D., Hauw, J.J. and Gold, G., 2002. Mixed dementia: epidemiology, diagnosis, and treatment. *Journal of the American Geriatrics Society*, *50*(8), pp.1431-1438.

Zhang, J. and Liu, F., 2014. Tissue-specific insulin signaling in the regulation of metabolism and aging. IUBMB life, 66(7), pp.485-495
Zhang, L., Zheng, H., Luo, J., Li, L., Pan, X., Jiang, T., Xiao, C., Pei, Z. and Hu, X., 2018. Inhibition of endothelial nitric oxide synthase reverses the effect of exercise on improving cognitive function in hypertensive rats. *Hypertension Research*, *41*(6), pp.414-425.

Zhang, Y. and Skolnick, J., 2005. TM-align: a protein structure alignment algorithm based on the TM-score. *Nucleic acids research*, *33*(7), pp.2302-2309.

Zhang, Y., Zhou, B., Zhang, F., Wu, J., Hu, Y., Liu, Y. and Zhai, Q., 2012. Amyloid-β induces hepatic insulin resistance by activating JAK2/STAT3/SOCS-1 signaling pathway. *Diabetes*, *61*(6), pp.1434-1443.

Zhang, X., Zhou, K., Wang, R., Cui, J., Lipton, S.A., Liao, F.F., Xu, H. and Zhang, Y.W., 2007. Hypoxia-inducible factor 1α (HIF-1α)-mediated hypoxia increases BACE1 expression and β-amyloid generation. *Journal of Biological Chemistry*, 282(15), pp.10873-10880.

Zhou, L., Barão, S., Laga, M., Bockstael, K., Borgers, M., Gijsen, H., Annaert, W., Moechars, D., Mercken, M., Gevaer, K. and De Strooper, B., 2012. The neural cell adhesion molecules L1 and CHL1 are cleaved by BACE1 protease in vivo. *Journal of Biological Chemistry,* 287(31), pp.25927-25940.

Zhou, P., Jin, B., Li, H. and Huang, S.Y., 2018. HPEPDOCK: a web server for blind peptide–protein docking based on a hierarchical algorithm. *Nucleic acids research*, *46*(W1), pp.W443-W450.

Zuliani, G., Cavalieri, M., Galvani, M., Passaro, A., Munari, M.R., Bosi, C., Zurlo, A. and Fellin, R., 2008. Markers of endothelial dysfunction in older subjects with late onset Alzheimer's disease or vascular dementia. *Journal of the neurological sciences*, *272*(1-2), pp.164-170.

Zuliani, G., Trentini, A., Rosta, V., Guerrini, R., Pacifico, S., Bonazzi, S., Guiotto, A., Passaro, A., Seripa, D., Valacchi, G. and Cervellati, C., 2020. Increased blood BACE1 activity as a potential common pathogenic factor of vascular dementia and late onset Alzheimer's disease. *Scientific reports*, *10*(1), pp.1-8.